Modeling Coupled Dynamic Processes in Wieringermeer Landfill Using Particle Filtering

By

Ioannis Charis
4314379

December 2016

Master of Science
Faculty of Civil Engineering and Geosciences
Geo-Engineering Track
Delft University of Technology

TU Delft

Title:	Modelling Coupled Dynamic Processes in Wieringermeer Landfill Using Particle Filtering
Author:	Ioannis Charis
Student number:	4314379
Date:	December 2016
Supervisor:	Prof. Dr. Ir. T. J. Heimovaara (TU Delft)
Thesis committee:	Dr. Phil. Vardon (TU Delft) Dr. G. Schoups (TU Delft) Ir. A.G. van Turnhour (TU Delft)
Postal address:	Civil Engineering and Geosciences Department Geo-Engineering Section Delft University of Technology Stevinweg 1 2628 CN Delft The Netherlands

Copyright ©2016 Section of Geo-Engineering

All rights reserved.
No parts of this publication may be reproduced,
Stored in a retrieval system, or transmitted,
In any form or by any means, electronic,
Mechanical, photocopying, recording, or otherwise,
Without the prior written permission of the
Section of Geo-Engineering of the Technical University of Delft

CONTENTS

1. Introduction 14
1.1. Project Overview 14
1.2. Research Questions 14
1.3. Thesis Organization 15
2. Theory 16
2.1. Landfill Description 16
2.2. Water Balance Model Description 17
2.2.1. Model Driving Mechanism 17
2.2.2. Comparative Data Set 17
2.2.3. Model Conceptual Framework 18
2.2.3.1. Cover Layer Model 19
2.2.3.2. Waste Body Model 20
2.3. Uncertainty Problem 24
2.4. Data Assimilation 26
2.4.1. Bayes' Theorem 26
2.4.2. State-Space Models 26
2.4.3. Particle Filtering 27
3. Materials and methods 31
3.1. Overview of Thesis Strategy 31
3.2. Uncertainty of Model States 31
3.3. Uncertainty of Model Parameters 33
3.4. Coupling PFSIR-PR Method and Water Balance Model 35
3.5. Implementation Tools 39
4. Results and Discussion 40
4.1. Assessment of Model States 40
4.1.1. Cumulative Leachate Outflow 41
4.1.2. Leachate Discharge Rate 42
4.1.3. Cover Layer Water Content 43
4.1.4. Water Infiltration 44
4.1.5. Waste Body Water Volume 46
4.2. Assessment of Model Parameters 48
4.3. Sensitivity Analysis 49
5. Conclusions and Future Work 58
Bibliography 60
Appendix A 65
Appendix B 66

List of figures

2.1. Location and aerial photograph of Wieringermeer landfill. 16
2.2. Situation of waste cells, leachate drainage and gas wells in Wieringermeer landfill. 16
2.3. Measured rainfall from the Berkhout station of the KNMI. 18
2.4. Measured potential evaporation from the Berkhout station of the KNMI. 18
2.5. Visualization of water balance model. 19
2.6. Schematic overview of the time-discretized domain of water balance model. 23
2.7. Schematic diagram of uncertain components in a computational model. 25
3.1. Comparison between simulated and measured cumulative leachate ouflow. 32
3.2. Comparison between simulated and measured leachate discharge rate. 32
3.3. Histogram of the DREAM-derived parameters. 34
3.4. Evolution of the DREAM-derived parameter values. 35
3.5. Coupling PFSIR-PR method and water balance model. 37
4.1. Simulated and measured cumulative leachate outflow. 42
4.2. Simulated and measured leachate discharge rate. 43
4.3. Simulated and measured cover layer water content. 44
4.4. Simulated and measured water infiltration. 45
4.5. Simulated and measured cumulative water infiltration. 45
4.6. Simulated and measured waste body water volume. 47
4.7. Histogram of the mean values of the PFSIR-PR resampled parameter particles. 48
4.8. Evolution of the parameter particles with PFSIR-PR. 49
4.9. Estimated states and parameters using scenarios 1 to 4 from Table 4.10. 53
4.10. Estimated states and parameters using scenarios 5 to 8 from Table 4.10. 55
4.11. Estimated states and parameters using scenario 10 from Table 4.10. 56
4.12. Estimated states and parameters using scenarios 11 to 12 from Table 4.10. 57

LIST OF TABLES

2.1. Sources of model uncertainty. 25
3.1. Selected state variables from the water balance model for the assimilation update. 31
3.2. Parameters of the water balance model. 33
3.3. Optimal DREAM-derived parameters selected to run the water balance model. 34
4.1. Case scenarios selected to run the water balance model with and without data assimilation. 40
4.2. Noise statistical properties selected to generate Gaussian random noises with respect to the state variables listed in the first column for the implementation of the PFSIR-PR method. 40
4.3. Overview of results related to the cumulative leachate outflow state. 41
4.4. Overview of results related to the leachate discharge rate state. 42
4.5. Overview of results related to the cover layer water content state. 43
4.6. Overview of results related to the water infiltration state. 44
4.7. Overview of results related to the waste body water volume state. 46
4.8. Mean values of the parameter particles obtained with the PFSIR-PR approach. 49
4.9. Noise statistical properties selected to generate Gaussian random noises with respect to the state variables listed in the first column for the implementation of the PFSIR-PR method. 51
4.10. Sensitivity analysis scenarios. 51
4.11. Sensitivity analysis results using scenarios 1 to 4 from Table 4.10 that relate to the cumulative leachate outflow state. 52
4.12. Sensitivity analysis results using scenarios 1 to 4 from Table 4.10 that relate to the leachate discharge rate state. 53
4.13. Sensitivity analysis results using scenarios 5 to 8 from Table 4.10 that relate to the cumulative leachate outflow state. 54
4.14. Sensitivity analysis results using scenarios 5 to 8 from Table 4.10 that relate to the leachate discharge rate state. 54
4.15. Mean values of the state variables simulated by the water balance model using case scenarios 1 and 2 from Table 4.1. 54
4.16. Mean values of the state variables simulated by the water balance model using case scenarios 3 and 4 from Table 4.1. 54
4.17. Minimum and maximum values of the parameter particles obtained with the PFSIR-PR approach using case scenarios 1 to 4 from Table 4.1. 54
4.18. Sensitivity analysis results using scenario 10 from Table 4.10 that relate to the cumulative leachate outflow and leachate discharge states. 55
4.19. Sensitivity analysis results using scenario 11 from Table 4.10 that relate to the cumulative leachate outflow and leachate discharge states. 56
4.20. Sensitivity analysis results using scenario 12 from Table 4.10 that relate to the cumulative leachate outflow and leachate discharge states. 56

List of algorithms

2.1. Solution of the cover layer model. 21
2.2. Solution of the wast body model. 25
2.3. Particle Filter Sequential Importance Sampling algorithm. 29
2.4. Particle Filter Sequential Importance Resampling algorithm. 30

LIST OF ABBREVATIONS

Acronym	Desctription
DA	Data Assimilation
DREAM	DiffeRential Evolution Adaptive Metropolis
KNMI	Koninklijk Nederlands Meteorologisch Instituut
MAE	Mean Absolute Error
MATLAB	MAtrix LABoratory
MSW	Municipal Solid Waste
pdf	propability distribution function
PF-SIR	Particle Filter Sequential Importance Resampling
PF-SIS	Particle Filter Sequential Importance Sampling
PFSIR-PR	Particle Filter Sequential Importance Resampling-Parameter Resampling
RMSE	Root Mean Square Error
SMC	Sequential Monte Carlo

NOMENCLATURE

Symbol	Desctription	Unit
α	Coefficient used in the perturbation of model parameters	-
β	Fast water flow fraction	-
δ	Dirac measure	-
Δz_{root}	Depth of vegetative cover layer	m
η_{t-1}	Noise of state vector at time t - 1	-
Θ	Parameter set of the water balance model	-
Θ_{t}^{i}	Particles of the parameter vector at time t	-
Θ_{t-1}^{i}	Particles of the parameter vector at time t - 1	-
$\bar{\Theta}_{t-1}^{i}$	Mean value of the parameter particles at time t - 1	-
θ	Modeled volumetric water content in the cover layer	-
θ_{est_t}	Estimated volumetric water content in the cover layer at time t	-
θ_r	Residual water content in the cover layer	-
θ_s	Saturated water content in the cover layer	-
θ_t	Modeled volumetric water content in the cover layer at time t	-
θ_{t-1}	Modeled volumetric water content in the cover layer at time t - 1	-
θ_t^i	Particles of the modeled volumetric water content in the cover layer at time t	-
θ_{t-1}^i	Particles of the modeled volumetric water content in the cover layer at time t - 1	-
θ_t'	Modeled volumetric water content in the waste body at time t	-
λ_t^i	Factor that describes the evolution of the parameter particles at time t	-
μ_{fast}	Mean residence time of the fast water flow in the waste body layer	days
μ_{slow}	Mean residence time of the slow water flow in the waste body layer	days
ρ	Landfill porosity	-
$\sigma_{\Theta_{t-1}'}$	Standard deviation values of the parameter particles at time t - 1	-
σ_e	Standard deviation of Gaussian noise	-
σ_y	Noise standard deviation of the measurement vector	-
σ_{fast}	Standard deviation of the residence time of fast water flow in the waste body layer	days
σ_{slow}	Standard deviation of the residence time of slow water flow in the waste body layer	days
τ	Water residence time in the waste body	days
$A_{landfill}$	Landfill area	ha/m^2
B	Boundary conditions	-
cdf_j	Lognormal cumulative distribution function	-
cdf_T	Largest value from the lognormal cumulative distribution function	-
C_{fact}	Factor that indicates the growth or decrease of vegetation at the cover layer	-
e_t	Noise of measurement vector at time t	-
$Exchange_t$	Exchange factor between the mobile and immobile water phase in the waste body at time t	-
Ev_{pot}	Measured potential evaporation	m/day
$f(\cdot)$	Bimodal lognormal function that describes the two phase distribution of water in the waste body	-
F^{-1}	Inverse of the cumulative probability distribution of the normalized particle weights	-

h_t	Non-linear function that describes the evolution of the measurement vector at time t	-
K_{sat}	Maximum hydraulic saturated conductivity in the cover layer	m/day
L_{max}	Maximum permitted pumping water level in the pump pit	m^3
L_{min}	Minimum permitted pumping water level in the pump pit	m^3
m	Empirical parameter used in the calculation of the water infiltration in the waste body	-
M	Model structure	-
$\mathcal{M}_t$	Forward model used to propagate the state variables one time step ahead	-
n	Number of days where the Particle Filter approach is applied	days
n''	Number of resampled particles	-
n_i'	Number of duplicated particles in the resampling step	-
N	Number of particles	-
$\mathcal{N}$	White Gaussian noise	-
pdf_j	Lognormal probability density function	-
$p(\Theta)$	Prior probability of the model parameter set	-
$p(x)$	Prior probability of the state vector	-
$p(x_0)$	Initial prior probability of the state vector at time t_0	-
$p(x_t)$	Prior probability of the state vector at time t	-
$p(x_t \mid x_{t-1})$	Transition density function of the hidden Markov Chain state	-
$p(x \mid y)$	Posterior probability of the state vector	-
$p(x_t \mid y_{1:t})$	Posterior probability of the state vector at the update step	-
$p(x_t \mid y_{1:t-1})$	Posterior probability of the state vector at the prediction step	-
$p(y_t \mid y_{t-1})$	Normalization factor in Bayes' law	-
$p(y \mid x)$	Likelihood function of the measurement vector	-
$p(y_t \mid x_t)$	Likelihood function of the measurement vector at time t	-
$p(\Theta, x_t \mid y_{1:t})$	Joint density function	-
q_{cum}	Modeled cumulative leachate outflow	m^3
q_{cum_t}	Modeled cumulative leachate outflow at time t	m^3
$q_{cum_{t-1}}$	Modeled cumulative leachate outflow at time t - 1	m^3
$q^i_{cum_t}$	Particles of the cumulative leachate outflow state at time t	m^3
$q^i_{cum_{t-1}}$	Particles of the cumulative leachate outflow state at time t - 1	m^3
q^{obs}_{cum}	Measured cumulative leachate outflow	m^3
$q^{obs}_{cum_t}$	Measured cumulative leachate outflow at time t	m^3
$q_{discharge}$	Modeled leachate discharge rate	m^3/day
$q_{discharge_t}$	Modeled leachate discharge rate at time t	m^3/day
$q_{discharge_{t-1}}$	Modeled leachate discharge rate at time t - 1	m^3/day
$q^i_{discharge_t}$	Particles of the leachate discharge rate at time t	m^3/day
$q^i_{discharge_{t-1}}$	Particles of the leachate discharge rate at time t - 1	m^3/day
$q^{obs}_{discharge}$	Measured leachate discharge rate	m^3/day
q_{ev}	Modeled potential evaporation	m/day
q_{ev_t}	Modeled potential evaporation at time t	m/day
q_{inf}	Modeled water infiltration into the landfill	m/day
q_{inf_t}	Modeled water infiltration into the landfill at time t	m/day
$q_{inf_{t-1}}$	Modeled water infiltration into the landfill at time t -1	m/day
q_{rf}	Measured rainfall	m/day
q_{rf_t}	Measured rainfall at time t	m/day
Q_{inf}	Modeled water infiltration into the waste body	m^3/day

Q_{inf_t}	Modeled water infiltration into the waste body at time t	m^3/day
$Q^i_{inf_t}$	Particles of the water infiltration state at time t	m^3/day
$Q^i_{inf_{t-1}}$	Particles of the water infiltration state at time t -1	m^3/day
RF	Measured rainfall	m/day
S	Modeled effective saturation in the cover layer	-
T	Days of water flow in the waste body	days
u	Model input values	-
u'	Uniforms generated in the systematic resampling step within the interval [0,1)	-
u_t	Non-linear function that describes the evolution of the state vector at time t	-
u_k	A single uniform generated in the resampling step	-
$\tilde{u}_k$	N number of uniforms generated in the resampling step within the interval [0,1)	-
$V_{landfill}$	Landfill volume	m^3
V_M	Modeled mobile volume of water in the waste body	m^3
V^1_M	First state in the discretized mobile water phase	m^3
V_{M_t}	Modeled mobile volume of water in the waste body at time t	m^3
$V_{M_{t-1}}$	Modeled mobile volume of water in the waste body at time t -1	m^3
$V^T_{M_t}$	Last state in the discretized mobile water phase at time t	m^3
$V^{1:T-1}_{M_t}$	First 1000 states in the discretized mobile water phase at time t	m^3
$V^{2:T}_{M_t}$	Last 1000 states in the discretized mobile water phase at time t	m^3
$V^j_{M_t}$	Total number of states in the discretized mobile water phase at time t	m^3
$V^j_{M_{t-1}}$	Total number of states in the discretized mobile water phase at time t -1	m^3
$V^i_{M_t}$	Particles of the mobile water volume state at time t	m^3
$V^i_{M_{t-1}}$	Particles of the mobile water volume state at time t -1	m^3
V_{IM}	Modeled imobile volume of water in the waste body	m^3
V_{IM_t}	Modeled imobile volume of water in the waste body at time t	m^3
$V_{IM_{t-1}}$	Modeled imobile volume of water in the waste body at time t -1	m^3
$V^i_{IM_t}$	Particles of the immobile water volume state at time t	m^3
$V^i_{IM_{t-1}}$	Particles of the immobile water volume state at time t -1	m^3
w_i	Particle weights	-
w^i_t	Particle weights at time t	-
w^k_t	Resampled particle weights at time t	-
x	State vector	-
x_0	Initial state vector at time t_0	-
x_i	Particles of the state vector	-
x_k	A single resampled state vector	-
x_t	State vector at time t	-
x_{t-1}	State vector at time t -1	-
$\hat{x}_t$	Filtered state vector at time t	-
x^i_t	Particles of the state vector at time t	-
x^i_0	Initial particles of the state vector at time t_0	-
x^k_t	Resampled particles of the state vector at time t	-
X	Hidden Markov Chain state	-
y	Measurement vector	-
y_t	Measurement vector at time t	-

Y	Series of measurements related to the hidden Markov Chain state	-

ACKNOWLEDGEMENTS

I would first like to thank my thesis advisor Prof. Dr. Ir. T. J. Heimovaara of the Civil Engineering and Geosciences department at the Delft University of Technology for his invaluable help and precious guidance. I have learnt many things since I became his student and more importantly, he stimulated and inspired me to obtain an irrational love for research.

I am also gratefully indebted to Dr. Ir. G. Schoups and Dr. P. Vardon from the Water Management and Geo-Engineering section of the Delft University of Technology, respectively. Without their participation and input, this master thesis could not have been successfully conducted.

I would also like to thank my daily supervisor Ir. A .G. van Turnhout from the Geo-Engineering section of the Technology University of Deft for his amicable and valuable suggestions that helped me to make a huge progress throughout this master thesis research.

Last but not the least important, I must express my very profound gratitude to my familly for providing me with priceless support and relentless encouragement throughout my years of study. This accomplishment would not have been possible without them. Thank you.

Ioannis Charis
Paris, France
December 2016

ABSTRACT

In antithesis of significant advances in environmental forecasting the last decades, the modeling of complex coupled processes in Municipal Solid Waste (MSW) landfills remains a challenging issue. In this context, a water balance model has been developed by Heimovaara et al. to describe the water flow through the Wieringermeer landfill (Northern Holland) and determine the amount of leachate produced. Despite that, the results yielded by this model provide compelling evidence that it is associated with a high degree of uncertainty. In this computational model, uncertainty is distinguished from the model parameters and estimates. Against this background, the central issue that motivates this research is to devise a simple approach to resolve the uncertainty problem in the water balance model. For this purpose, this study presents a robust Particle Filter Sequential Importance Resampling method with parameter resampling (PFSIR-PR). In this method, the parameters evolve over time and are estimated along with the state variables without the need to obtain observations for all of them. In addition, the problem of parameter impoverishment is overcome by perturbing the parameters based on the kernel smoothing principle. The performance of this approach is evaluated using multiple well-known quantitative measures. The results indicate that the proposed technique can successfully illustrate the intricate landfill dynamics and alleviate model uncertainties. As a consequence, the PFSIR-PR approach has made the water balance model an effective tool for modelling complicated processes in sanitary landfills.

1 INTRODUCTION

1.1. Project Overview

Dynamics of natural systems are studied with models that simulate the states under interest with the use of governing equations. These equations rely on the intrinsic and extrinsic properties of the explored systems and are represented by a set of parameters in a model structure. It is generally agreed today that such sophisticated models often fail to estimate reliable state variables. Uncertain model outputs frequently arise from incorrect input data, inappropriate model formulation, and improperly defined model parameters.

The water balance model (Hemovaara et al. 2015) was devised to delineate the complex interplay of physical, chemical and biological processes that occur within the Wieringermeer landfill. The model aims to predict the water infiltration into the landfill, the landfill volume of water, and the leachate outflow from the landfill outlet. However, as it will be seen, there is a noticeable discrepancy between the simulated model outputs and real landfill data which is an indication that there is some uncertainty linked to the model itself.

Much attention has been directed towards addressing the issue of uncertainty in prediction models. To solve this problem, several data assimilation methods have been proposed that are used to merge observations into model predictions. Among existing data assimilation methods, the Particle Filter has attracted considerable attention for applications to hydrological modelling [Moradkhani (2005b); Moradkhani (2012); Plaza (2012); Plaza (2013); Vrugt (2013)], occeanography [Mattern (2013)], environmental studies [Chang and Li (2007); Chang (2012)], and robotics [Thrun (2002); Rekleitis (2004)].

The Particle Filter approach was originally developed to handle dynamic non-linear or/and non-Gaussian models by correcting uncertain model states. However, it is important to note that a number of studies have shown the need to obtain parameter values consistent with data-assimilated states [Andrieu (2004); Carvalho (2010)]. This concept has been clearly demonstrated by Nagarajan et al. (2010), Chang et al. (2012) and Moradkhani et al. (2012) extending the application of the Particle Filter approach for the estimation of model parameter values.

In the current study, we aim to minimise the uncertainty associated with the states and parameters of the water balance model. To achieve that, the performance of the PFSIR-PR approach is applied to the water balance model for estimating the model state variables along with the model parameters.

1.2. Research Questions

The intention of this master thesis research is to ameliorate the performance of the water balance model by estimating accurate model states and parameters. To accomplish that, the problem of model uncertainty should be effectually resolved. For this reason, the present study must give a clear-cut answer to the questions listed below:

- Which are the sources of uncertainty that have adverse effects on the water balance model?
- Which of them can be effectively tackled?

- How is it possible to deal with them?

To sup up the foregoing, this research will initially explore whether and to which extent the model parameters and states, the model structure, and the model forcing data cause the model uncertainty. Then, the study examines the applicability of the proposed data assimilation method to the unreliable model sources. And finally, this dissertation applies a powerful data assimilation method to reduce the uncertainty in the water balance model by correcting the unreliable model sources.

1.3. Thesis Organization

This master thesis report is structured as follows:

- Section 1 throws light on the background and purpose of this master thesis project
- Section 2 gives a precis of the literature study
- Section 3 includes a detailed description of the methods applied in this research
- Section 4 summarises the results of this study
- Section 5 draws the conclusions

2 THEORY

2.1. Landfill Description

As shown in Fig. 2.1, the Wieringermeer landfill is located in the north-west of the Netherlands. The landfill is divided into a western and eastern part. The western part was exploited since 2001. In contrast, the operation of the eastern part started in 1985 and ended in 2000.

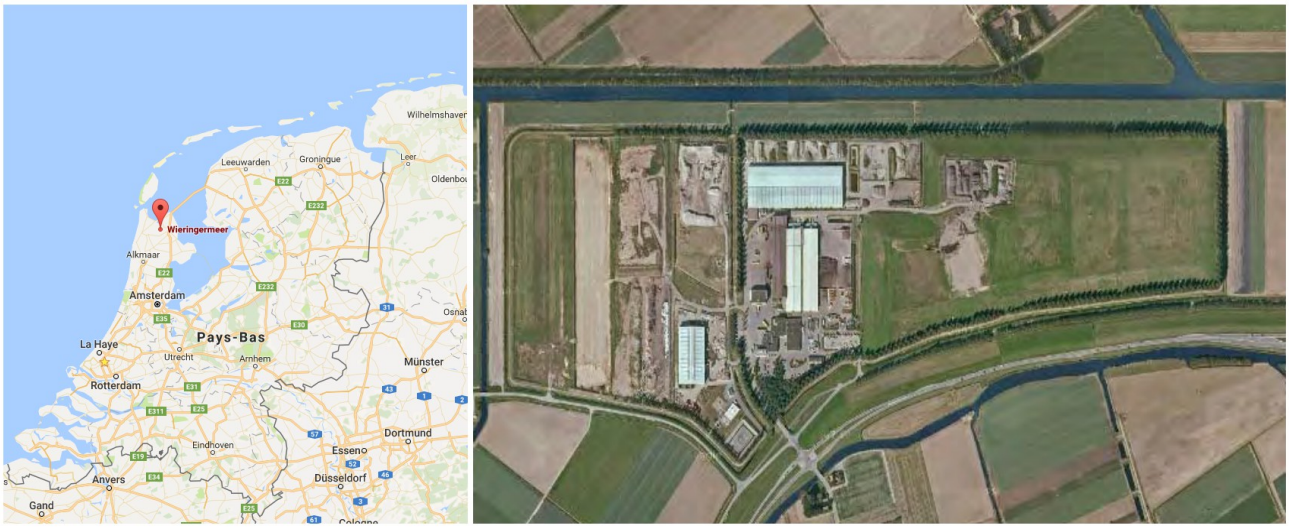

Fig. 2.1: Location and aerial photograph of Wieringermeer landfill (Meeteren et al. 2009).

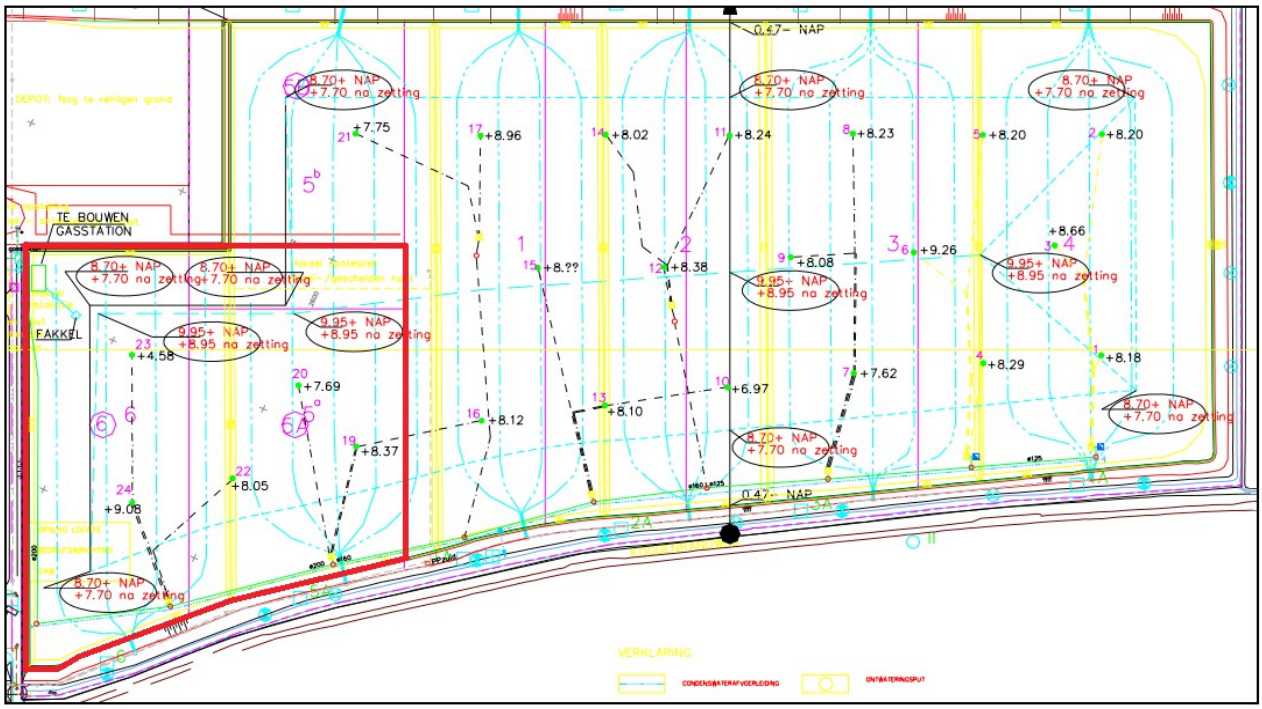

Fig. 2.2: Situation of waste cells, leachate drainage and gas wells in Wieringermeer landfill (Meeteren et al. 2009).

The height of the eastern part is at about 12 meters whilst the surface area is 19 hectare (ha) divided into 6 compartments. All these compartments have a bottom liner, a leachate drainage system, a gas drainage system and settlement beacons, as indicated in Fig. 2.2. Waste cells 2 to 4 have an impermeable top layer in contrast to the other cells that are covered with a layer of soil at around 1.5 meters. At this point, it is worth noting that this research focused on modeling the processes that occur in cells 5a and 6 of the inactive eastern part of this landfill using measured data of the leachate quantity. Cells 5a and 6 are illustrated as a red-marked cell in Fig. 2.2.

2.2. Water Balance Model Description

The investigated water balance model delineates the water flow through the Wieringermeer landfill by coupling processes such as rainfall, evapotranspiration, infiltration, and leachate drainage. In addition, measurements are used for driving the model and comparatively evaluating the model outputs. More details regarding this computational model are given below.

2.2.1. Model Driving Mechanism

Data collection in support of operating prediction models is of vital importance. In this study, the water balance model is based on daily rainfall and potential evaporation measurements that work as a driving mechanism for this model. Although site based measurements were available, we chose to use rainfall and potential evaporation data from the closest observing station found almost 15 km (Berkhout, North Holland) away from the landfill. It is clear that this choice may have a noticeable impact on the model output.

Figs. 2.3 and 2.4 show daily rainfall ([RF m/day]) and potential evaporation ([Ev_{pot} m/day]) measurements, respectively. These measurements are obtained from the Berkhout weather station of the Royal Netherlands Meteorological Institute (i.e. Koninklijk Nederlands Meteorologisch Instituut or in short form KNMI), for the period 23 March 1999 to 23 June 2016. From these figures, it can be seen that the rainfall is evenly distributed over time. In addition, it is evident that evaporation exceeds rainfall in summer that in turn denotes seasonal patterns of rainfall infiltration into the waste body of the Wieringermeer landfill.

2.2.2. Comparative Data Set

In this research, simulated leachate discharge and cumulative leachate outflow were compared with real measurements to evaluate the performance of the water balance model with and without data assimilation[1]. The cumulative leachate outflow was measured from 25 May 2012 to 1 May 2016 with a 15-minute interval. The measured leachate discharge rate was derived as the gradient of the measured cumulative leachate outflow on a daily basis.

[1]Leachate is measured as cumulative leachate outflow $\left(q_{cum}^{obs}\ [\text{m}^3]\right)$ and leachate discharge rate $\left(q_{discharge}^{obs}\ [\text{m}^3/\text{day}]\right)$.

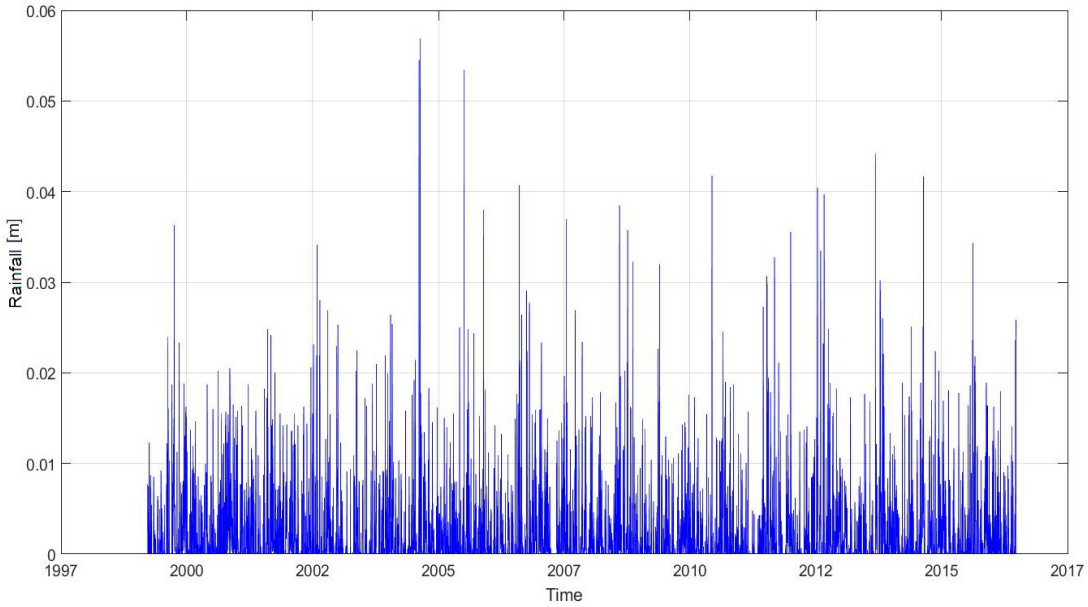

Fig. 2.3: Measured rainfall from the Berkhout station of the KNMI.

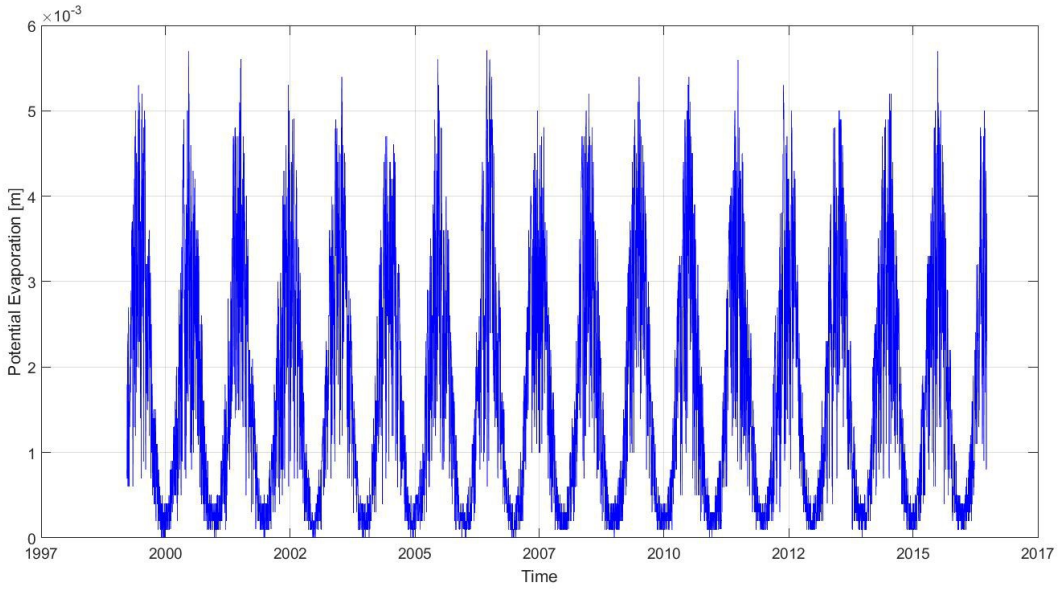

Fig. 2.4: Measured potential evaporation from the Berkhout station of the KNMI.

2.2.3. Model Conceptual Framework

The water balance model consists of three different sub-models, each describing a layer of the landfill system. Fig. 2.5 illustrates that the model (Heimovaara et al. 2015) is comprised of three layers: a top layer of soil and grass, the waste body, and the leachate collection system; i.e. drainage well.

The model is based on the assumption that rainwater (q_{rf} [m/day]) initially infiltrates into the vegetative cover layer from where some amount either evaporates (q_{ev} [m/day]) or gradually moves downward into the waste body layer (q_{inf} [m/day]). As the water trickles through the waste body, it dissolves chemicals and other particles, creating leachate[1].

[1]Leachate is simulated as cumulative leachate outflow $(q_{cum}\,[\,\mathrm{m^3}])$ and leachate discharge rate $(q_{discharge}\,[\,\mathrm{m^3/day}\,])$.

Subsequently, it is hypothesized that a small amount of this liquid follows preferential flow paths towards the drainage layer fast enough where the remainder accumulates in the waste body. The assumption is that the longer the water remains in the waste body, more solutes can diffuse into the water from the bulk of the waste.

As a consequence, the pumped leachate $\left(q_{cum}^{obs}\right)$ represents the quantitative information concerning the cumulative leachate outflow. In reality, the leachate present in the drainage layer is daily pumped from the pump pit installed in close proximity to the landfill.

As illustrated in Fig. 2.5, if the pumped leachate level is higher than a predefined level (L_{max}) then the pump pit ceases to collect the drained leachate. Instead, if the pumped leachate level is below (L_{max}) the pump pit continues to pump out the leachate from the drainage well. Nevertheless, the pump pit is not allowed to pump more leachate than a preconcerted level (L_{min}). The time scale of storage in the drainage layer was shown to be very small, that it was disregarded for the remainder of this study.

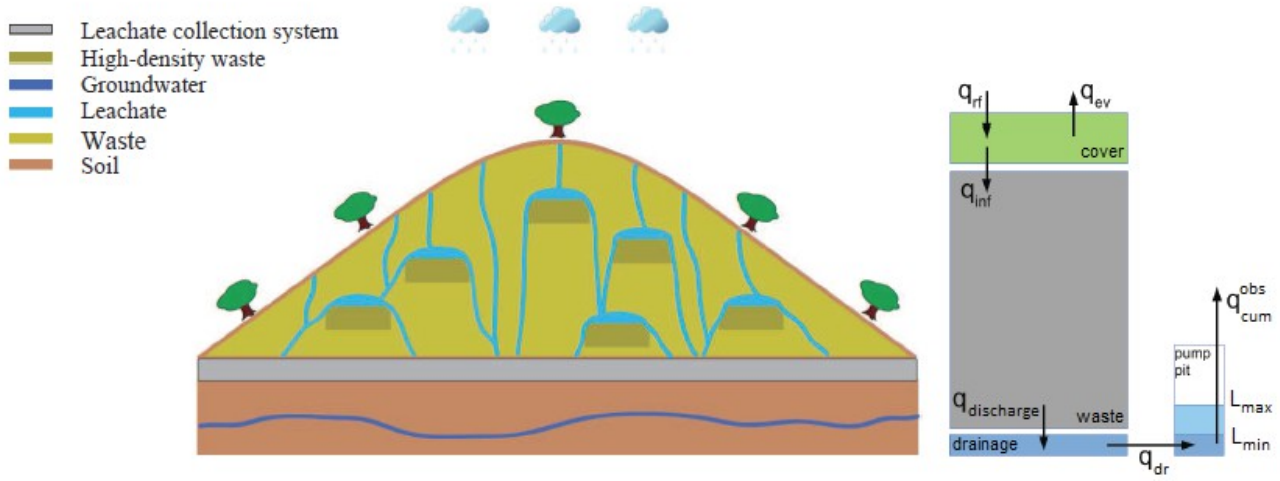

Fig. 2.5: Visualization of water balance model (Heimovaara, 2015; Konstantaki, 2015).

2.2.3.1. Cover Layer Model

The cover layer is defined by the mass balance equation, as such (Heimovaara et al. 2015):

$$\frac{\partial \theta}{\partial t} = \nabla \cdot q + Evaporation \quad (1)$$

The discretization of Equation (1) leads to:

$$\frac{\Delta \theta}{\Delta t} = \frac{q_{rf} - q_{inf}}{\Delta z_{root}} + \frac{q_{ev}}{\Delta z_{root}} \quad (2)$$

In equation (2), θ represents the volumetric water content, Δt denotes the time step used for the model which is defined by the measurement frequency of the rainfall and potential evaporation data. The flows q_{rf}, q_{inf} and q_{ev} are the rainfall, infiltration and evaporation flux in m/day, the rooting depth Δz_{root} is considered to be

equal to the depth of the cover layer from which evaporation can occur. The infiltration flux is by definition based on an empirical power law relationship given by:

$$q_{inf} = -K_{sat} \cdot S^{m},\ 0 \leqslant S \leqslant 1 \quad (3)$$

Here, K_{sat} is defined as the maximum saturated hydraulic conductivity in m/day, m is an empirical parameter, and S represents the effective saturation that is defined as:

$$S = \frac{\theta - \theta_r}{\theta - \theta_s},\ 0 \leqslant \theta \leqslant \theta_s \quad (4)$$

Where θ_s and θ_r illustrate the saturated and residual water contents, respectively. This implies that when the water content is equal or smaller than the residual water content the water ceases to sink into the waste body layer by gravity. Next, equation (5) shows that the evaporation flux is computed based on the potential evaporation data provided by the KNMI (Ev_{pot}) multiplied by a crop factor C_{fact} that takes into account the average effect of the vegetative cover layer.

$$q_{ev} = Ev_{pot} \cdot C_{fact} \quad (5)$$

The mass balance of the cover layer is solved based on the discretized form of equation (2) assuming a single layer and a daily time step. To guarantee that the new water content will not move out from the interval $0 \leq \theta_t \leq \theta_{t\text{-}1}$, the following considerations are taken into account as shown in Algorithm 2.1[1].

2.2.3.2. Waste Body Model

Heimovaara et al. (2015) model the water flow through the waste body with a transfer function approach [Jury and Roth (1990); Zacharof and Butler (2004a,b); Rosqvist and Destouni (2000); Rosqvist (2005)] expressed as:

$$q_{discharge}(t) = \int_0^{\infty} q_{inf}(t-\tau) \cdot f(\tau) d\tau \quad (12)$$

The hypothesis is that two different types of water flow develop within the waste body (Heimovaara, et al. 2015). It is assumed that the water flows through the waste body are slow or fast resulting in a distribution of residence times. This two-phase distribution is described by a bimodal lognormal function as:

$$f(\cdot) = f(\tau, \mu_{fast}, \sigma_{fast}, \mu_{slow}, \sigma_{slow}) = \frac{\beta}{\tau \cdot \sigma_{fast} \cdot \sqrt{2 \cdot \pi}} \cdot e^{\frac{-(\ln(\tau) - \ln(\mu_{fast}))^2}{2 \cdot \sigma_{fast}^2}} + \frac{1-\beta}{\tau \cdot \sigma_{slow} \cdot \sqrt{2 \cdot \pi}} \cdot e^{\frac{-(\ln(\tau) - \ln(\mu_{slow}))^2}{2 \cdot \sigma_{slow}^2}} \quad (13)$$

In equation (13), β and β-1 represent the fraction of the fast and slow water flow distributions, respectively. Furthermore, τ denotes the residence time of the water in the waste body. In addition, μ_{fast}, μ_{slow}

[1] In Algorithm 2.1, Θ illustrates the total set of model parameters.

illustrate the mean residence times of the fast and slow flow water and σ_{fast}, σ_{slow} are the standard deviations of the lognormal distributions, respectively.

Algorithm 2.1: Solution of the cover layer model (Heimovaara et al. 2015).

$[\theta_t, q_{inf_t}]$ = CoverLayerModel(θ_{t-1}, $q_{inf_{t-1}}$, RF, Ev_{pot}, Θ)

1. The infiltration flux is estimated at time t based on the water content from the previous time-step t-1:

$$q_{inf_t} = -K_{sat} \cdot S(\theta_{t-1})^m \quad (6)$$

Then, the water content at time t is calculated as follows:

$$\theta_{est_t} = \theta_{t-1} - (q_{rf_t} - q_{inf_t} + q_{ev_t}) \cdot \frac{\Delta t}{\Delta z_{root}} \quad (7)$$

2. If $\theta_{est_t} > \theta_s$ the cover layer is saturated and the excess water immediately drains into the waste body layer as such:

$$q_{inf_t} = q_{inf_t} + (\theta_s - \theta_{est_t}) \cdot \frac{\Delta z_{root}}{\Delta t} \quad (8)$$

Next, θ_{est_t} is recalculated based on equation (7).

3. Else if $\theta_{est_t} < 0$ and $\theta_{t-1} > \theta_r$, it illustrates that excessive amount of water has infiltrated into the waste body layer or evaporated from the cover layer. Therefore, the water quantity that enters the waste body layer is limited as follows:

$$q_{inf_t} = (\theta_r - \theta_{t-1}) \cdot \frac{\Delta z_{root}}{\Delta t} \quad (9)$$

In this case, θ_{est_t} is also recomputed with equation (7).

4. If $\theta_{est_t} < 0$, it denotes that the evaporation rate is overestimated and is corrected with:

$$q_{ev_t} = q_{ev_t} + \theta_{est_t} \cdot \frac{\Delta z_{root}}{\Delta t} \quad (10)$$

In a manner similar to the previous steps, θ_{est_t} is re-estimated by using equation (7).

5. In the end, the updated value of the water content is defined equal to the estimated one:

$$\theta_t = \theta_{est_t} \quad (11)$$

Fig. 2.6 outlines the time-discretized domain of the waste body model. The total water volume in the waste body of the Wieringermeer landfill consists of a mobile water volume (V_M [m^3]) and an immobile water volume (V_{IM} [m^3]).

To exemplify, counting from the last to the first cell; i.e. from right to left as sketched in Fig. 2.6, the water present in the first cell of this discretized scheme will flow first out of the waste body entering the leachate collection system as shown above. Conversely, the water stored in the last cell will reach at the landfill outlet after 1000 days.

In the light of the aforementioned considerations, it follows that at every time step, the leachate discharge rate equals the first waterlogged cell from the discretized domain of the mobile water phase as expressed below

$$q_{discharge_t} = V^1_{M_t} \quad (14)$$

Whereas, the cumulative leachate outflow is estimated as such:

$$q_{cum_t} = q_{discharge_t} + q_{discharge_{t-1}} \quad (15)$$

Equation (15) indicates that q_{cum} is computed as the cumulative sum of $q_{discharge}$ between two time steps *t* and *t*-1. All the while, as it was indicated in Fig. 2.5, the pump pit continues pumping out the concentrated leachate from the drainage well.

In the same manner, counting once again from the last to the first cell, the flowing water stored in each cell jumps from one cell to another as time moves from a time period *t*-1 to the next *t*. This process is described by the next equation:

$$V^j_{M_t} = V^j_{M_{t-1}} + Q_{inf_t} \cdot pdf_j \quad (16)$$

In which, $j = 1,...,T$ represents each individual cell or the corresponding flow day from this discretized domain and Q_{inf_t} [m^3/day] denotes the real amount of water distributed into the entire landfill, which is obtained at every time period *t* as such:

$$Q_{inf_t} = q_{inf_t} \cdot A_{landfill} \quad (17)$$

In Equation (17), q_{inf_t} is the modeled infiltration of water into the landfill with a unit of measurement in m/day, and $A_{landfill}$ is the total area of the Wieringermeer landfill in m^2.

Thereafter, based on these assumptions, the portion of water that seeps into the landfill is daily introduced into the mobile water domain in descending order (i.e. from the highest value at the first cell to the smallest value at the last cell) with the aid of the next equation:

$$pdf_j = \frac{\beta}{\tau \cdot \sigma_{fast} \cdot \sqrt{2 \cdot \pi}} \cdot e^{\frac{-(\ln(\tau) - \ln(\mu_{fast}))^2}{2 \cdot \sigma_{fast}^2}} + \frac{1-\beta}{\tau \cdot \sigma_{slow} \cdot \sqrt{2 \cdot \pi}} \cdot e^{\frac{-(\ln(\tau) - \ln(\mu_{slow}))^2}{2 \cdot \sigma_{slow}^2}} \qquad j = 1,...,T \quad (18)$$

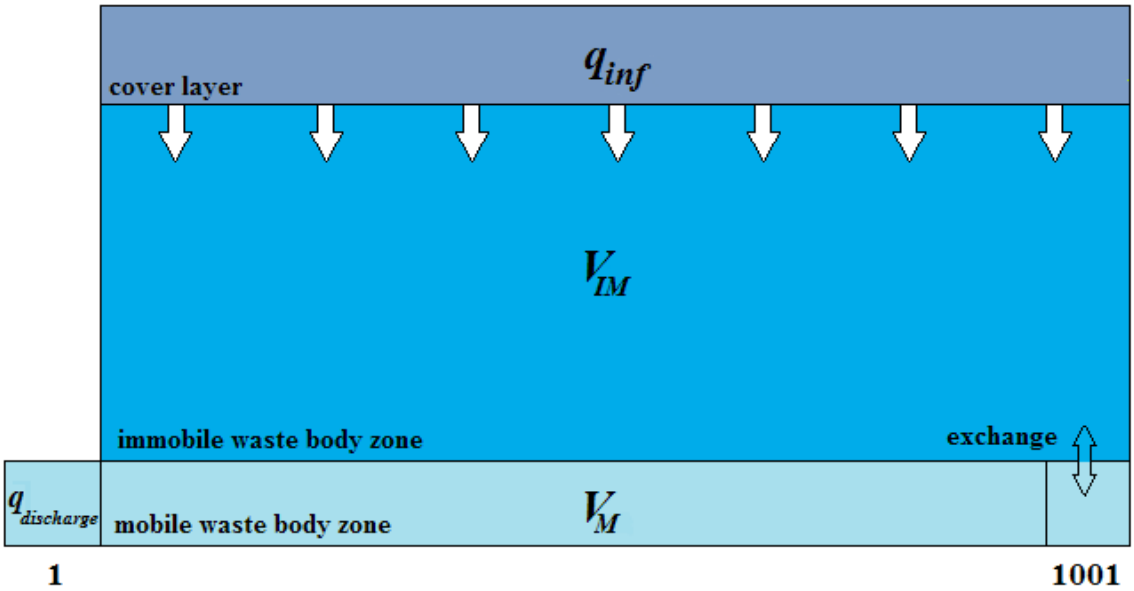

Fig. 2.6: Schematic overview of the time-discretized domain of water balance model.

In which, $\tau = \{\tau_1, ..., \tau_T\} = \{1, ..., T\}$ indicates the 1001 number of water flow days. Following an analogue assumption for the immobile water content, it is assumed that the immobile water volume propagates forward in time according to:

$$V_{IM_t} = V_{IM_{t-1}} + Q_{inf_t} \cdot (1 - cdf_T) \quad (19)$$

In this case, Q_{inf} is added to the motionless landfill water based on:

$$cdf_j = \beta \cdot \int_0^{\tau} \frac{e^{\frac{-(\ln(t) - \ln(\mu_{fast}))^2}{2 \cdot \sigma_{fast}^2}}}{\tau} d\tau + (1-\beta) \cdot \int_0^{\tau} \frac{e^{\frac{-(\ln(\tau) - \ln(\mu_{slow}))^2}{2 \cdot \sigma_{slow}^2}}}{\tau} d\tau \quad (20)$$

Here, equation (20) is the same as equation (13) but now in its cumulative form, which means that only a scant fraction $1 - cdf_T$ of Q_{inf} is allocated to the immobile water quantity at every time step.

In parallel, it is assumed that there is a diffusive exchange between the mobile and immobile water phase that is formulated in terms of the last mobile cell $V_{M_t}^T$ and the single cell of the immobile water (V_{IM_t}). This exchange is described as follows.

Initially, the volumetric water content θ'_t in the waste body is calculated at every new time step t, as shown below:

$$\theta_t^{'} = max\left(\frac{V_{IM_t}}{V_{landfill}}\right) \quad (21)$$

In equation (21), $V_{landfill}$ represents the landfill volume in m^3. With this in mind, it can be deduced that V_{IM} represents the remaining amount of water in the waste body. Next, the exchange between the mobile and immobile water phase is given by:

$$Exchange_t = min\left(K_{sat} \cdot A_{landfill} \cdot \left(\frac{\theta_t^{'}}{\rho}\right)^m, V_{M_t}^T\right) \quad (22)$$

Eventually, the mobile and immobile water volumes are updated based on the following considerations. Primarily, the exchange factor calculated in equation (22) is subtracted from the immobile water quantity as follows:

$$V_{IM_t} = V_{IM_t} - Exchange_t \quad (23)$$

Finally, the cells of the mobile water domain are shifted such that the outflow of the first cell into the drainage well is taken into account. The first cell is removed and replaced by the second cell of the mobile water domain at every new time-step. Furthermore, the last cell of the same domain is set to be equal to the above-computed exchange factor. These assumptions are described by the next equations:

$$V_{M_t}^{1:T-1} = V_{M_t}^{2:T} \quad (24)$$

$$V_{M_t}^T = Exchange_t \quad (25)$$

The afore-described waste body model is written in a pseucode form in Algorithm 2.2.

2.3. Uncertainty Problem

Broadly speaking, computational models are almost always prone to some level of uncertainty. On the whole, unreliable model outputs emanate from various doubtful sources. As of today, it is broadly recognized that the uncertainty of models is usually caused by the factors visualized in Fig. 2.7 and listed in Table 2.1. From these types of uncertainty, the boundary conditions and the initial states are frequently regarded as a part of the model structure and input data set, respectively.

Numerous studies of uncertainty analysis in computational models report that among these uncertainty components, five of them; i.e. B, u, x_0, Θ, and M, are considered the sources that result in the uncertain model states; i.e. x [Regan (2002); Y. Liu and Gupta (2007); Uusitalo (2015)].

To put it another way, it can be understandable that the model outputs are evidently represented by the state variables. On that account, the maximal reduction of the uncertainty associated with a prediction model can be achieved by adequately correcting B, u, x_0, Θ, and M before running the model. In doing so, reliable

model outputs are likely to be obtained. More notably, this is accomplishable by means of up-to-date data assimilation techniques that are discussed in detail below.

Algorithm 2.2: Solution of the waste body model (Heimovaara et al. 2015).

$[q_{cum_t}, q_{discharge_t}, V_{IM_t}]$ = WasteBodyModel($q_{cum_{t-1}}, q_{discharge_{t-1}}, V_{IM_{t-1}}, RF, Ev_{pot}, \Theta$)

1. Calculate the lognormal probability and cumulative density function using equations (18) and (20), respectively.
2. Obtain the water infiltration into waste body from the cover layer model in Algorithm 2.1:

   $[\theta_t, q_{inf_t}]$ = CoverLayerModel(θ_{t-1}, $q_{inf_{t-1}}$ RF, Ev_{pot}, Θ)

   -FOR t = 1, 2,...
3. Multiply the simulated from the cover layer model water infiltration by the landfill area, such as in equation (17).
4. Propagate forward in time the mobile and immobile water quantities according to equations (16) and (19), respectively.
5. Calculate the leachate discharge rate and the cumulative leachate outflow based on equations (14) and (15), respectively.
6. Estimate the water content in the waste body given by equation (21).
7. Compute the exchange between the mobile and immobile water quantities according to equation (22).
8. Update the mobile and immobile volumes of water according to equations (23), (24) and (25).

-END FOR

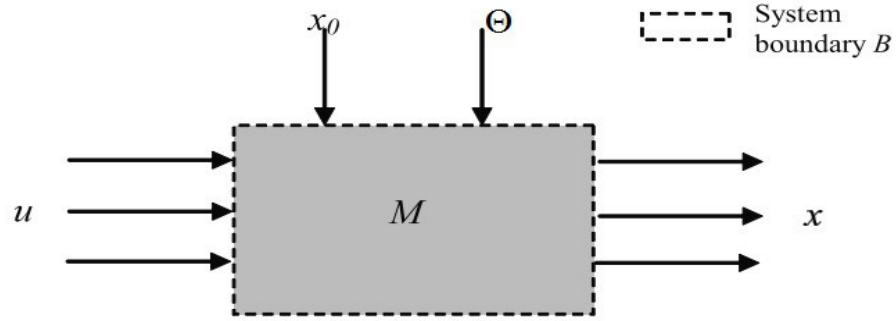

Fig. 2.7: Schematic diagram of uncertain components in a computational model (Y. Liu and Gupta 2007).

Table 2.1: Sources of model uncertainty.

Symbols	Uncertainty factors
B	Boundary conditions
u	Inputs
x_0	Initial states
Θ	Parameters
M	Model structure
x	State variables

2.4. Data Assimilation

Data assimilation is considered as a blending of model and data that facilitates the reliable estimation of model states or/and parameters. Data assimilation schemes establish a concrete connection between uncertain model variables and parameters and allow estimating them from incomplete measurements of all or some of them. In particular, a meaningful and harmonic reconciliation between imperfect model results and error-prone measurements can be obtained through this modern technique.

A review of the literature suggests that there are a plethora of data assimilation methods [Arulampalam (2002); Chen (2003)]. In the following sections, it will be seen that this research gravitates towards the Particle Filter approach that has its origin in Bayesian estimation and is therefore discussed first.

2.4.1. Bayes' Theorem

Bayes' theorem provides the fundamental foundation for data assimilation. In actual fact, data assimilation exploits available observations obtained from a system under investigation to optimize the model that describes the system of interest. In probability theory and statistics, these considerations are expressed by means of a probability distribution function (pdf) that attempts to estimate a value x given an observation y [Leeuwen (2009); Leeuwen (2010)]. In the Bayesian inference scheme, this is written as:

$$p(x \mid y) = \frac{p(y \mid x) \cdot p(x)}{\int p(y \mid x) \cdot p(x)\, dx} \quad (26)$$

Where $p(x \mid y)$ denotes the posterior probability of x. In addition, $p(y \mid x)$ is defined as the likelihood that represents the probability that the data y, is likely to be produced by means of x. Also, $p(x)$ is known as the prior distribution of x, when the observation y is not taken into account. In the end, the denominator is termed the normalization factor, which guarantees that the probability density $p(x \mid y)$ integrates to 1. It is important to realize that the solution to the data assimilation problem given by equation (26) is not an inverse problem, but a simplified multiplication problem.

2.4.2. State-Space Models

In state estimation problems, the state vector x that contains all model variables, and the vector y that represents the quantitative information regarding x, evolve forward in time according to the next equations [Doucet (2000); Arulampalam (2002); Chen (2003)]:

$$x_t = f(x_{t-1}, u_t, \eta_{t-1}) \quad (27)$$

$$y_t = f(x_t, h_t, e_t) \quad (28)$$

Alternatively, equations (27) and (28) are written as:

$$x_t = x_{t-1} + u_t + \eta_{t-1} \quad (29)$$

$$y_t = x_t \cdot h_t + e_t \quad (30)$$

Here, x_t and x_{t-1} denote the state vector at time t and t-1, respectively. In addition, y_t is the measurement vector at time t. Meanwhile, u_t and h_t illustrate the non-linear functions that describe the evolution of the state and measurement vector at time t, respectively. Furthermore, η_{t-1} and e_t represent the error added in the estimates of x_{t-1} and y_t, respectively.

The state-space formulation of the data assimilation problem can be intimately combined with Bayes' theorem. In fact, it is well-known that a state space model is comprised of two sequences of random variables:

1) The hidden state X~x_t forming a Markov chain with transition density $p(x_t|x_{t-1})$ at every time step *t.* Where the transition density is described by the state vector equation; i.e. equation (27) or (29).

2) A series of observations Y~$y_{1:t}$ with probability density $p(y_t|x_t)$ that is dependent on the hidden Markov chain state.

The data assimilation problem revolves around the question how to incorporate all the observed information to give an estimate of the latent process. In this respect, the main objective in Bayesian filtering is to approximate the posterior probability of x_t given the observations $y_{1:t}$ that is expressed as $p(x_t|y_{1:t})$ and is recursively estimated in two steps (Olivier et al. 2007):

1) The prediction step:

$$p(x_t|y_{1:t-1}) = \int p(x_{t-1}|y_{1:t-1}) \cdot p(x_t|x_{t-1}) dx_{t-1} \quad (31)$$

2) The update step:

$$p(x_t|y_{1:t}) = \frac{p(x_{t-1}|y_{1:t-1}) \cdot p(y_t|x_t)}{\int p(x_t|y_{1:t-1}) \cdot p(y_t|x_t) dx_t} \quad (32)$$

In the present study, the Particle Filter approach was preffered to approximate the posterior $p(x_t|y_{1:t})$ and is presented below.

2.4.3. Particle Filtering

Particle Filtering is a sequential Monte Carlo (SMC) method that approximates the posterior probability of x_t using $i = 1,...,N$ number of particles with associated weights. Primarily, based on the SMC principles, the prior distribution of X is described as:

$$p(x_t) = \frac{1}{N} \cdot \sum_{i=1}^{N} \delta \cdot (x_t - x_t^i) \quad (33)$$

Here, δ denotes a Dirac measure that is commonly defined as :

$$\delta_x(\mathrm{X}) = \begin{cases} 0 & if\ x \in \mathrm{X} \\ 1 & if\ x \notin \mathrm{X} \end{cases} \quad (34)$$

At this point, it is impracticable to draw particles inasmuch as the posterior $p(x_t | y_{1:t})$ is unknown. In spite of this, new particles can be drawn from a known importance pdf based on prior knowledge of the system. This is the basis of the Particle Filter Sequential Importance Sampling (PF-SIS) approach, which is illustrated in Algorithm 2.3. Under these assumptions, the insertion of equation (33) into equation (26) leads to [Leeuwen (2009); Leeuwen (2010)]:

$$p(x_t | y_{1:t}) = \sum_{i=1}^{N} w_t^i \cdot \delta \cdot (x_t - x_t^i) \quad (35)$$

In this way, the particle description of the posterior $p(x_t | y_{1:t})$ is obtained. The derivation of equation (35) is more rigorously explained in appendix A of this document. In what follows, w_t^i is given by:

$$w_t^i = \frac{p(y_t | x_t^i)}{\sum_{v=1}^{N} p(y_t | x_t^v)} \quad (36)$$

In equation (36), w_t^i denote the weights associated with the particles. Then, the weights are normalized as such:

$$w_t^i = \frac{w_t^i}{\sum_{i=1}^{N} w_t^i} \quad (37)$$

With these particles and their associated weights, the filtered state vector is usually estimated as the mean of the posterior $p(x_t | y_{1:t})$ and is expressed as (Arulampalam et al. 2002):

$$\hat{x}_t = \sum_{i=1}^{N} x_t^i \cdot w_t^i \quad (38)$$

However, it should be mentioned that a noteworthy limitation of the importance sampling principle is the fact that the variance of weights can only increase over time (Doucet et al. 2001), which results in the degeneracy phenomenon. This degeneracy implies that after some time almost all the particles will have insignificant weights affecting the accuracy of results.

A simple but effective way of tackling this degeneracy problem is to apply resampling during the filtering process (Gordon et al. 1993). The resampling step is used to generate $k = 1,...,N$ number of new

particles (x_t^k) and weights (w_t^k) at every time step. Resampled particles (x_t^k) having high weights (w_t^k) are used to replace particles with low weights (x_t^i). The literature on the resampling scheme indicates that several methods exist to resolve the so-called degeneracy problem [Kitagawa (1996); Carpenter (1999); Doucet (2000); Douc (2005); Hol (2006)]. The most commonly used resampling methods are presented below:

Algorithm 2.3: Particle Filter Sequential Importance Sampling algorithm.

1. Initialize at time $t = 0$ by drawing $i = 1,...,N$ number of particles x_0^i from the prior distribution $p(x_0)$.

-FOR $t = 1$ to n
-FOR $i = 1$ to N

2. Propagate the particles according to equation (29).
3. Calculate the weights based on (36).
4. For each particle x_t^i assign a weight w_t^i.

-END FOR

5. Normalize weights given by (37).
6. Calculate the filtered state using (38).

-END FOR

1) Multinomial resampling:

Generate $k = 1,...,N$ ordered uniform independent numbers (u_k) as such:

$$u_k = u_{k+1} \cdot \tilde{u}_k^{\frac{1}{N}} \quad (39)$$

In which, $\tilde{u}_k \sim U[0, 1)$. Subsequently, the resampled state particles are selected according to the following multinomial distribution:

$$x_k = x\left(F^{-1}(x_i)\right) \quad (40)$$

Where F^{-1} is the inverse of the cumulative probability distribution of the normalized particle weights.

2) Stratified resampling:

In this resampling method, the uniforms are generated as follows:

$$u_k = \frac{(k-1)+\tilde{u}_k}{N} \quad (41)$$

Thereafter, the state particles are resampled based on the multinomial distribution presented above.

3) Systematic resampling:

In this approach, the uniforms are drawn as given below:

$$u_k = \frac{(k-1)+u'}{N} \quad (42)$$

In equation (42), u' ~ U[0, 1). After that, the resampled particles are found using the above mentioned multinomial distribution.

4) Residual resampling:

This specific resampling scheme generates $n_i' = \lfloor N \cdot w_i \rfloor$ duplicates of particle x_i to the new distribution. Here, $\lfloor \ \rfloor$ denotes the integer part. After this, $n'' = N - \sum n_i'$ particles are resampled from x_i. In this case, the selection of x_i is proportional to $w_i = N \cdot w_i - n_i'$ and is effectuated by making use one of the previously mentioned resampling techniques.

Given these points, the insertion of the resampling step into the PF-SIS algorithm leads to the well-known Particle Filter Sequential Importance Resampling (PF-SIR) algorithm that is illustrated in Algorithm 2.4.

Algorithm 2.4: Particle Filter Sequential Importance Resampling algorithm.

1. Initialize at time $t = 0$ by drawing $i = 1,...,N$ number of particles x_0^i from the prior distribution $p(x_0)$.

-FOR $t = 1$ to n

-FOR $i = 1$ to N

2. Propagate the particles according to equation (29).
3. Calculate the weights based on (36).

-END FOR

5. Normalize weights given by (37).
6. Resample particles using one of the resampling methods described above.
7. Update state vector based on the resampled particles.
8. Update the filtered state as the mean of the resampled particles.

-END FOR

3 MATERIALS AND METHODS

3.1. Overview of Thesis Strategy

In this section we show how the uncertainty in the water balance model can be effectively reduced. For this reason, a robust data assimilation method is proposed to minimise the uncertain factors in the model and improve the model predictions. Firstly, it is of major importance to identify what are the causes of model uncertainty. Moreover, it is an intriguing issue to determine which of these unreliable model sources are likely to be tackled.

We chose not to change the model structure (M) due to the complexity of changing the conceptual framework of the water balance model. Consequently, we did not redefine the model boundary conditions (B), nor did we modify the meteorological forcing data of this model. However, the impact of these inputs (u) on the model outcome will be examined in detail. The main uncertainties we did consider are the initial states (x_0), the model parameters (Θ), and the state variables (x). A detailed examination of how these factors impact upon the reliability of the water balance model is presented below.

3.2. Uncertainty of Model States

As indicated in Table 3.1, the water balance model simulates the water content of the vegetative cover layer, the water infiltration into the waste body, and the landfill mobile and immobile water volumes, respectively. In addition, the cumulative leachate outflow and the leachate discharge rate are both derived from the mobile water volume as shown in Section 2.

Table 3.1: Selected state variables from the water balance model for the assimilation update.

Order	Symbol	Description	Unit	Class†
1	θ	Cover layer water content	-	V
2	q_{cum}	Cumulative leachate outflow	m^3	V_0
3	$q_{discharge}$	Leachate discharge rate	m^3	V_0
4	Q_{inf}	Water infiltration into the waste body	m^3/day	V
5	V_{IM}	Waste body immobile water content	m^3	V
6	V_M	Waste body mobile water content	m^3	V

† The class V and V_0 illustrate the unobservable and observable state variables, respectively.

With no doubt, Figs. 3.1 and 3.2 provide confirmatory evidence that the simulated from the water balance model states q_{cum} and $q_{discharge}$ are not in compliance with the measurements. In a nutshell, it can be deduced that these states are subject to uncertainty and should undoubtedly be corrected. This implies that the water balance model is a poorly calibrated model.

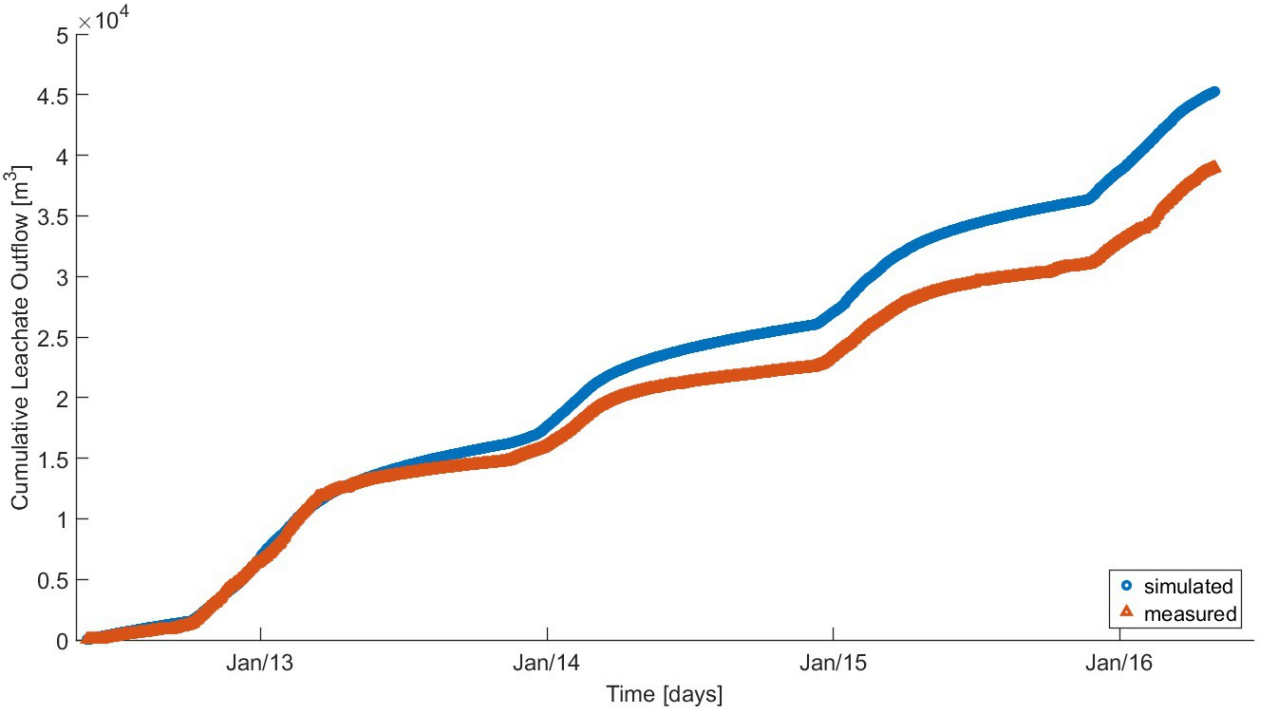

Fig. 3.1: Comparison between simulated and measured cumulative leachate ouflow.

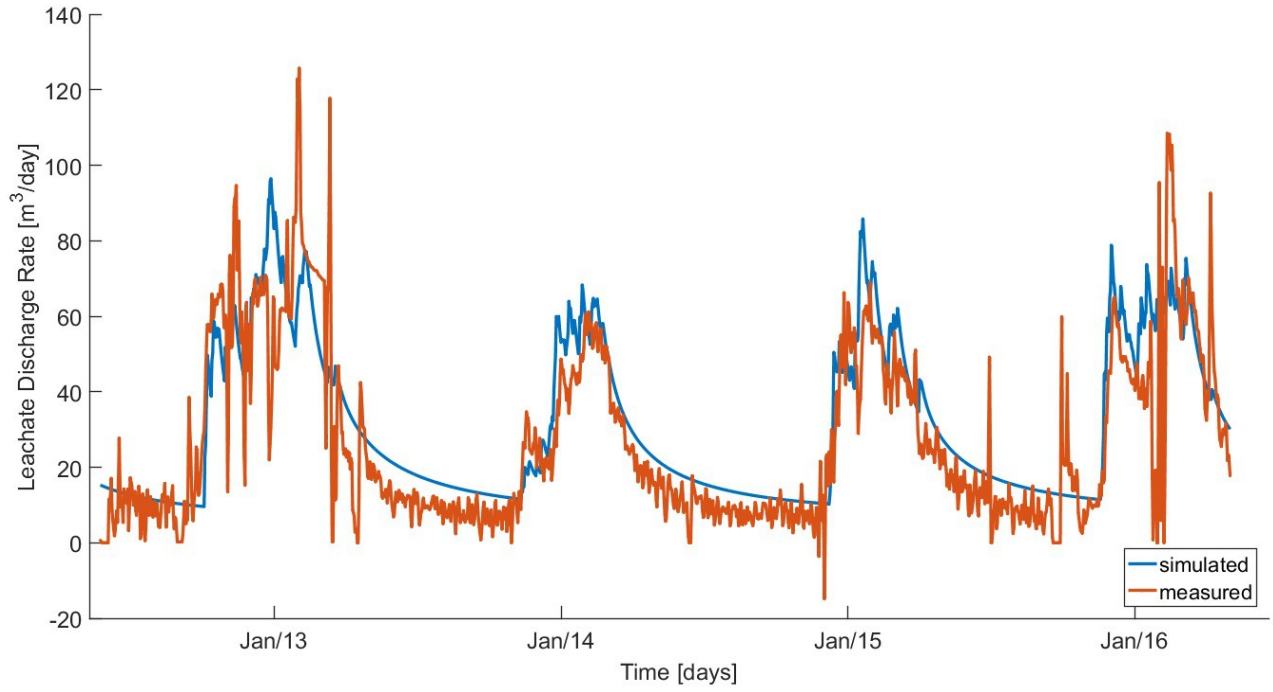

Fig. 3.2: Comparison between simulated and measured leachate discharge rate.

Now, it is worthwhile to remember that all the state variables are described by equations coupled to each other, as shown in section 2. To put it briefly, the interconnectedness between the states produced by the water balance model attests that not only the measured but also the unmeasured states are open to doubt. Therefore, in order to take into account the bias arising from all the dynamically combined states, each state listed in

Table 3.1 should be corrected through the proposed model-data reconciliation technique. Further insight into the interrelation between the simulated states is included in appendix B of this report.

3.3. Uncertainty of Model Parameters

It is known that all models have parameters that must be estimated. To run the water balance model, a Θ = 12 number of unknown parameters have to be found a priori. The parameters of water balance model are demonstrated in Table 3.2. In this context, Heimovaara, et al. preferred to calibrate these parameters through the model performance optimization that is effectuated by comparing simulated and measured cumulative leachate outflow data. In actuality, this was achieved by utilizing the robustness of the stochastic optimization technique DREAM [Laloy and Vrugt (2012); Vrugt (2015)] which is based on the Bayesian inference scheme. In fact, this approach approximates the posterior distribution of parameters. More specifically, having as a basis a prior parameter density $p(\Theta)$ the parameter inference contemporaneously with the model state trajectory is achieved by using inference of the joint density $p(\Theta, x_t | y_{1:t})$. By doing so, acceptable and reasonable values of parameters describing the simulated and measured data set are likely to be obtained.

Table 3.2: Parameters of the water balance model.

Order	Symbol	Description	Unit
1	Δz_{root}	Depth of the vegetative cover layer	m
2	C_{fact}	Factor that assesses the growth or decrease of the vegetative cover layer	-
3	θ_r	Residual water content in the cover layer	-
4	θ_s	Saturated water content in the cover layer	-
5	K_{sat}	Maximum saturated hydraulic water content in the cover layer	m/day
6	m	Empirical parameter used in equation (3)	-
7	μ_{fast}	Mean residence time of the fast water flow in the waste body layer	days
8	σ_{fast}	Standard deviation of the residence time of the fast water flow in the waste body layer	days
9	μ_{slow}	Mean residence time of the slow water flow in the waste body layer	days
10	σ_{slow}	Standard deviation of the residence time of the slow water flow in the waste body layer	days
11	β	Fast water flow fraction	-
12	$A_{landfill}$	Landfill area	ha/m^2

In this study, 150000 model evaluations were invoked where DREAM provided nearly 40000 different parameter sets. From these estimated parameters, Figs 3.3 and 3.4 unveil that C_{fact}, μ_{slow}, σ_{slow}, β, and $A_{landfill}$ appear to be normally distributed and have been converged to a specific value. Quite the reverse, the remaining parameters markedly deviate from a normal distribution and do not seem to reach convergence.

Table 3.3: Optimal DREAM-derived parameters selected to run the water balance model.

Δz_{root}	C_{fact}	θ_r	θ_{sat}	K_{sat}	m	μ_{fast}	σ_{fast}	μ_{slow}	σ_{slow}	β	$A_{landfill}$
[m]	[-]	[-]	[-]	[m/day]	[-]	[days]	[days]	[days]	[days]	[-]	[ha]
0.42	1.01	0.06	0.64	-6.5	4.52	-3.27	0.06	3.79	0.6	0.19	4.63

At this point, it should be mentioned that the best average description of the calibrated parameter values are chosen to run the model (see Table 3.3). However, as alluded to previously, the model simulations are not satisfying by making use of these fixed parameter values. Consequently, it can be concluded that the parameters selected to run the model may induce great effects on the model outputs. To overcome the uncertainty that stems from the model parameters, it might be advisable to run the model using various parameter sets in an attempt to pinpoint those parameter values that result in the best performing model. Nevertheless, the countless parameter sets provided by DREAM and the fact that some of the parameters pellucidly remain unconverged may render this process practically unattainable.

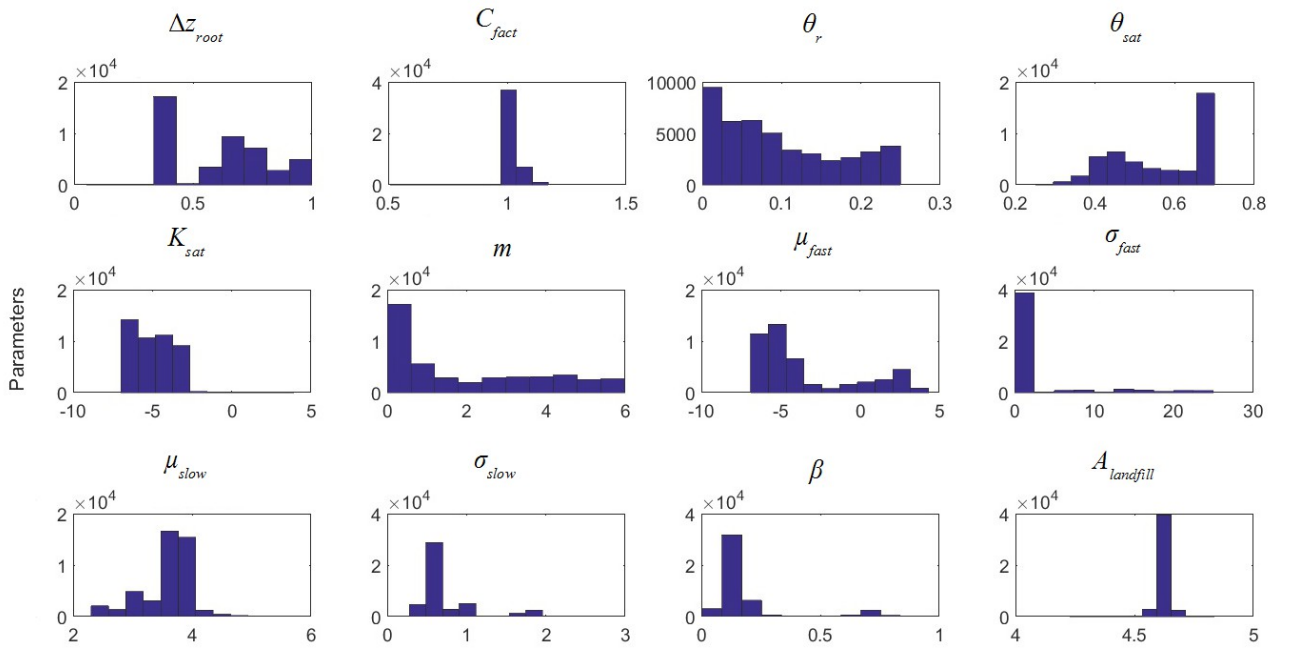

Fig. 3.3: Histogram of the DREAM-derived parameters.

As aforesaid, unchanged parameter values are used to run the water balance model. However, this choice is clearly wrong as the system of interest undergoes continuous evolution over time. A comprehensive view of this issue suggests that the investigated landfill environment is apparently a dynamic system. In fact, this hypothesis does not remain unverifiable taking into consideration the varying amount of water that enters the landfill or the overall complex endogenous landfill mechanisms. Under all these considerations, the present study will endeavour to obtain consistent parameter values with the states of interest, treating the DREAM-derived parameters as time-varying quantities through the following data assimilation method.

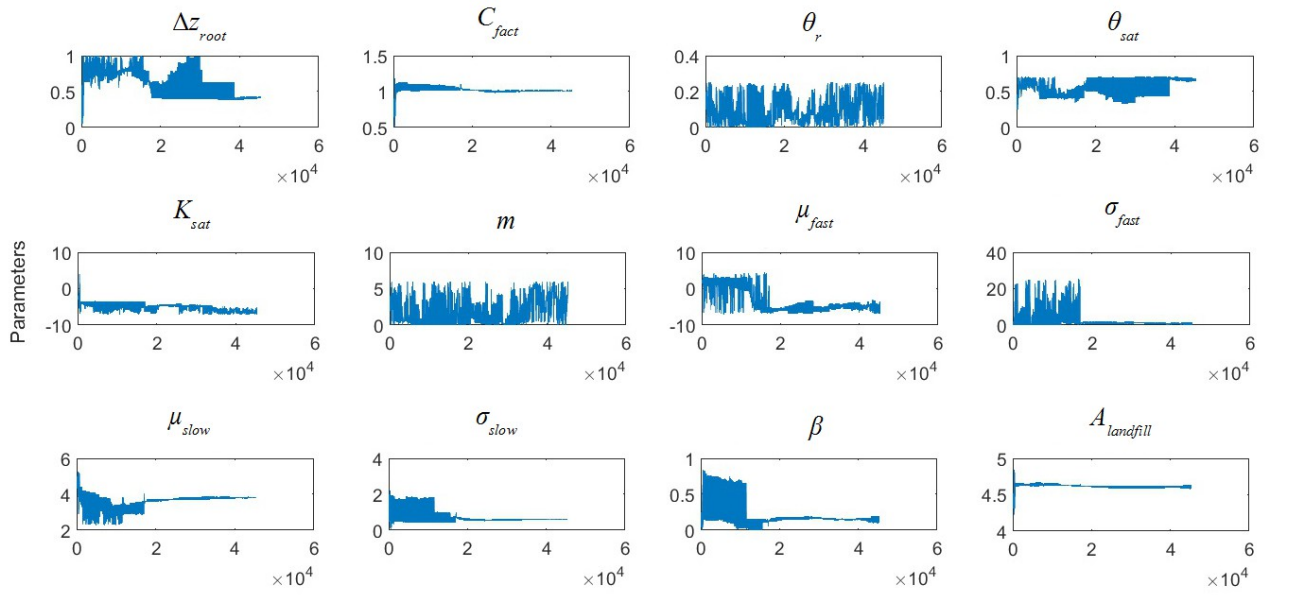

Fig. 3.4: Evolution of the DREAM-derived parameter values.

3.4. Coupling PFSIR-PR Method and Water Balance Model

The Particle Filter method presented here is reminiscent of the one proposed by Plaza et al. (2012) that focuses on the joint state-parameter estimation, which is, however, fundamentally dissimilar to former state-parameter estimation methods. The key idea behind this approach is to couple the states and parameters so as to found the best performing model estimates. More specifically, the proposed methodology relies on the interconnectedness between states and parameters, which are both estimated without the need to obtain observations for all of them. To this end, the PFSIR-PR approach is applied to the water balance model where observed and unobserved states are resampled along with parameters. Following this, the resampled parameters are perturbed to avoid extreme parameter replication. Against this backcloth, at each time step the model is run using these perturbed parameters in an attempt to identify an appropriate blend between the measured states, unmeasured states, and the model parameters. Given this orientation, the proposed methodology is illustrated in Fig. 3.5 that is detailedly elucidated as follows:

Step 1: First of all, N number of parameter values are sampled from the last 10000 values offered by DREAM. Thereby, reasonable parameter values close to their converged estimates are obtained.

Step 2: Afterwards, the water balance model is run by using the parameter values sampled in step 1. In this way, N number of simulated state values are obtained. These estimated state values synthesize the initial state vector x_0 at time t_0. Note that the state vector x and correspondingly the initial state vector x_0, consist of the uncertain model states presented in Table 3.1. Moreover, the initial time t_0 corresponds to the first day of measurement of the volume of drained leachate (i.e. 25 May 2012). Given these points, the state vector can be vectorized as follows:

$$x_t = \begin{bmatrix} \theta_t^i \\ q_{cum_t}^i \\ q_{discharge_t}^i \\ Q_{inf_t}^i \\ V_{IM_t}^i \\ V_{M_t}^i \end{bmatrix} \quad (43)$$

Step 3: In what follows, the PFSIR-PR approach is applied to the water balance model. Provided that, for i = 1,...,*N* number of particles and time step *t* = 1,...,*n*, the particle description of the model state vector evolves forward over time according to the next equation:

$$x_t = \underbrace{\begin{bmatrix} \theta_t^i \\ q_{cum_t}^i \\ q_{discharge_t}^i \\ Q_{inf_t}^i \\ V_{IM_t}^i \\ V_{M_t}^i \end{bmatrix}}_{x_t} = \underbrace{\begin{bmatrix} \theta_{t-1}^i \\ q_{cum_{t-1}}^i \\ q_{discharge_{t-1}}^i \\ Q_{inf_{t-1}}^i \\ V_{IM_{t-1}}^i \\ V_{M_{t-1}}^i \end{bmatrix}}_{x_{t-1}} + \underbrace{\left[\mathcal{M}_t\right]}_{u_t} + \underbrace{\begin{bmatrix} \eta_{1_t} \\ \eta_{2_t} \\ \eta_{3_t} \\ \eta_{4_t} \\ \eta_{5_t} \\ \eta_{6_t} \end{bmatrix}}_{\eta_t} \quad (44)$$

In which, $\mathcal{M}_t$ denotes the coupled water balance model; i.e. cover layer and waste body model, which propagates forward in time the particles of the state vector. At the same time, randomly distributed Gaussian noise is introduced to the state vector indicating the uncertainty in these forecasts. To this end, $\eta_{1_t}, \ldots, \eta_{6_t}$ illustrate the insertion of Gaussian noise to each state variable in equation (44). In the end of Step 3, if the current time step corresponds to a data assimilation event, Steps 4 to 7 are implemented. Otherwise, Step 3 is continuously performed until data are available.

Step 4: In this particular step, the particle weights are estimated given by:

$$w_t^i = \frac{1}{\sqrt{2\pi \cdot \sigma_y}} \cdot e^{\frac{-(x_t - y_t)^2}{2 \cdot \sigma_y^2}} \quad (45)$$

Here, x_t and y_t denote the state and measurement vector, respectively. In addition, σ_y is the standard deviation of measurement noise. In this regards, the measurement vector consists of the measured cumulative leachate outflow data. As aforementioned, the real quantitative information regarding the leachate outflow is given by means of the measured cumulative leachate outflow. Instead, the measured leachate discharge rates are empirically estimated as the gradient of the real measured data q_{cum}^{obs}. Therefore, this research preferred to assimilate the real pumped amount of leachate q_{cum}^{obs} into the corresponding modeled state q_{cum}.

Thereby, in the case presented here, x_t and y_t correspond to q_{cum} and q_{cum}^{obs} respectively. In addition, σ_y represents the noise standard deviation of q_{cum}^{obs}. After that, these weights are normalized based on equation (37).

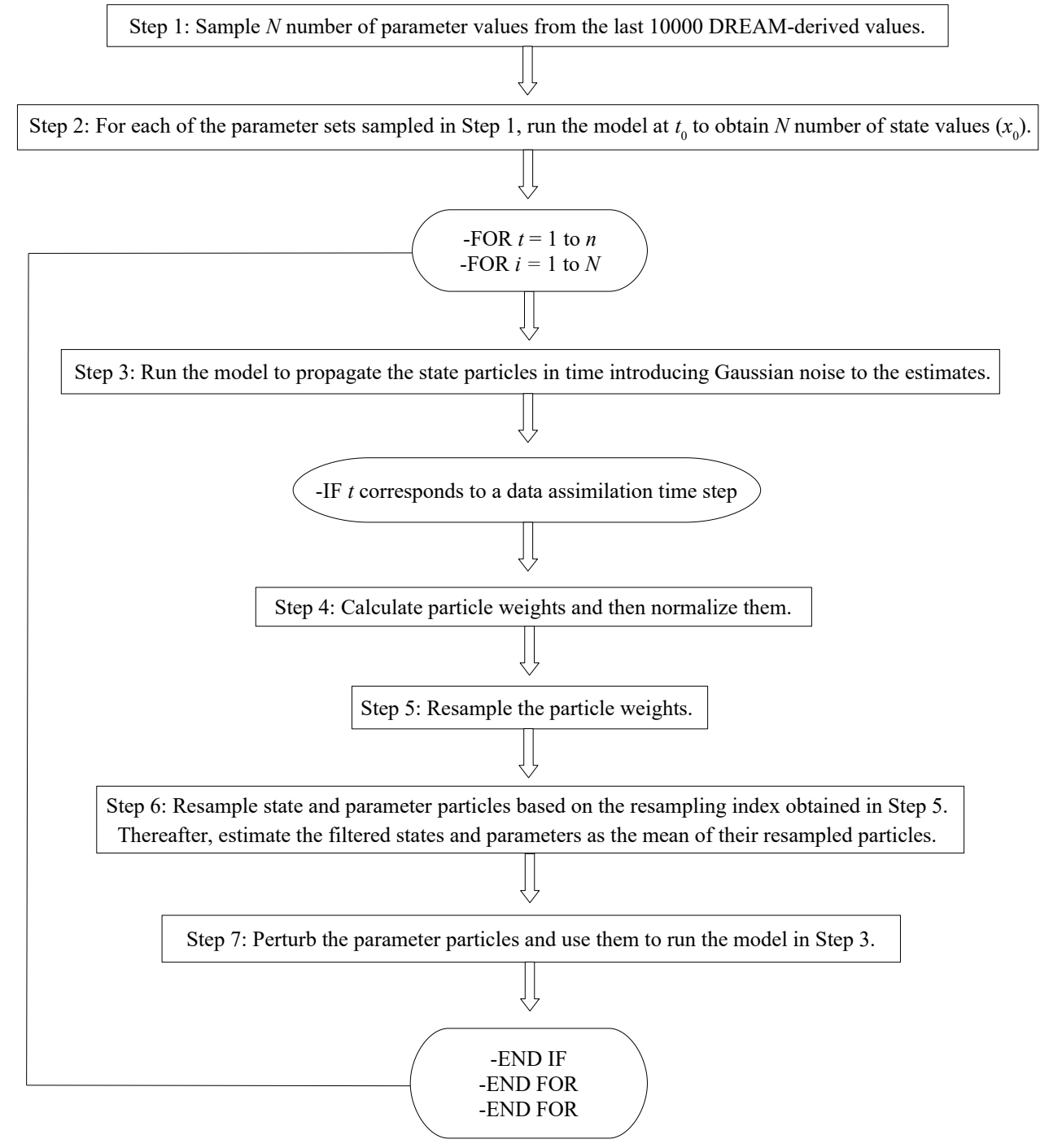

Fig. 3.5: Coupling PFSIR-PR method and water balance model.

Step 5: Thereafter, the weights are resampled using the multinomial resampling method. It is worth pointing out that the resampling step is introduced in order to exclude the possibility of encountering the degeneration problem throughout the data assimilation process.

Step 6: Following this, the state and parameter particles are resampled. This is actually done by means of the vector that includes the indices that are used to resample the weights. Thereby, these indices are used to resample the state and parameter particles. Afterwards, the filtered values of q_{cum} are obtained as the mean of their resampled particles. In a roundabout way, the unobserved state variables and the model parameters are also filtered by estimating the mean of their resampled particles. In this manner, the filtered unobserved state and parameter values are tied to the best possible realization of the data assimilated state; i.e. q_{cum}.

Step 7: In the final step of this methodology, the resampled parameters are perturbed. This action gives surety that the parameter values will not replicate in an extreme manner throughout the data assimilation operation. To date, various methods have been developed and introduced to perturb the model parameters while a data assimilation approach is applied to the model states. In any parameter perturbation technique, new values of parameter particles at each time step t (Θ_t^i) are obtained by adding an artificial evolution factor λ_t^i to the parameter samples of the previous step t-1 (Θ_{t-1}^i). This process is commonly described as such:

$$\Theta_t^i = \Theta_{t-1}^i + \lambda_t^i \quad (46)$$

In the traditional PFSIR-PR approach, the parameter samples are perturbed by adding random Gaussian noise $\lambda_t^i \sim N(0,\sigma_e)$ with zero mean and standard deviation σ_e, at each time step (Plaza et al. 2012). In this parameter perturbation approach, equation (46) is written as follows:

$$\Theta_t^i = \Theta_{t-1}^i + N(0,\sigma_e) \quad (47)$$

According to Plaza et al. (2012), σ_e is usually defined as a fraction of the optimal parameter value. However, it is apparent that this approach does not seem to be valid when the optimal parameter values are unknown or open to doubt. In this respect, this study has chosen to use the following parameter perturbation equation that has been proposed by J. Liu and West (2001).

$$\Theta_t^i = \alpha \cdot \Theta_{t-1}^i + (1-\alpha) \cdot \bar{\Theta}_{t-1}^i + \sqrt{1-\alpha^2} \cdot N(0,\sigma_{\Theta_{t-1}^i}) \quad (48)$$

In which, $\alpha = (3\delta-1)/2\delta$, δ is a factor in (0 1], Θ_t^i and Θ_{t-1}^i are the parameter particles at time t and t-1, respectively, and finally, $\bar{\Theta}_{t-1}^i$ and $\sigma_{\Theta_{t-1}^i}$ denote the mean and the standard deviation values of the parameter samples at time t-1, respectively.

The approach presented in equation (48) has been used by Moradkhani et al. (2005a), Erol et al. (2013) and Hu et al. (2014). More analytically, this method is based on the kernel smoothing algorithm which is a combination of parameter shrinkage and perturbation. In fact, in equation (48), $\alpha \cdot \Theta_{t-1}^{i} + (1-\alpha) \cdot \bar{\Theta}^{i}_{t-1}$ is the shrinkage term that decreases the parameters variance in the population of particles. On the other hand, $\sqrt{1-\alpha^2} \cdot N(0, \sigma_{\Theta_{t-1}^{i}})$ is the perturbation term that is introduced to the particle parameters values in an attempt to increase the variance of the particle parameter values.

Overall, the combination of parameter shrinkage and perturbation guarantees to keep the values of the parameter particles within reasonable limits (Hu et al. 2016). With the completion of these steps, the perturbed parameter values are used to run the water balance model and update the particles of the state vector at the next time step.

3.4. Implementation Tools

The afore-described algorithm; i.e. PFSIR-PR, was developed and applied to the water balance model in MATLAB R2016a (Version 9.0) software. In addition, the Microsoft Excel tool was used to store large volumes of data for the purpose of this master thesis research.

4 RESULTS AND DISCUSSION

4.1. Assessement of Model States

This section evaluates the results of the PFSIR-PR approach with respect to the uncertain model states. Data assimilation is performed on a daily and weekly basis, with the first data assimilation event at 25 May 2012 and the last at 1 May 2016. The reference water balance model without data assimilation is performed with the parameter set demonstrated in Table 3.3. Recall that the parameters listed in Table 3.3 are not optimally calibrated. The PFSIR-PR approach with parameter perturbation is performed by drawing $N = 50$ and $N = 100$ state and parameter particles. In sum, the reference model is run with and without data assimilation for each case listed in Table 4.1. After a trade-off analysis, the statistical properties listed in Table 4.2 are selected to draw Gaussian random noise that is introduced to the state variables at daily time steps.

Table 4.1: Case scenarios selected to run the water balance model with and without data assimilation.

Case 1	The PFSIR-PR approach is performed using daily DA events and $N = 50$ particles, while Gaussian noise generated according to the statistical properties listed in Table 4.2 is introduced to the state variables.
Case 2	The PFSIR-PR approach is performed using weekly DA events and $N = 50$ particles, while Gaussian noise generated according to the statistical properties listed in Table 4.2 is introduced to the state variables.
Case 3	The PFSIR-PR approach is performed using daily DA events and $N = 100$ particles, while Gaussian noise generated according to the statistical properties listed in Table 4.2 is introduced to the state variables.
Case 4	The PFSIR-PR approach is performed using weekly DA events and $N = 100$ particles, while Gaussian noise generated according to the statistical properties listed in Table 4.2 is introduced to the state variables.
Case 5	The reference model is run without DA using the parameter set listed in Table 3.3.

Table 4.2: Noise statistical properties selected to generate Gaussian random noises with respect to the state variables listed in the first column for the implementation of the PFSIR-PR method.

State	NMV†	NSDV‡	Unit
θ	0	0	-
q_{cum}	0	80	m^3
$q_{discharge}$	0	1	m^3/day
Q_{inf}	0	1	m^3/day
V_{IM}	0	10	m^3
V_{M}	0	0.2	m^3

†NM is the noise mean.

‡NSD is the noise standard deviation.

In this analysis, the Mean Absolute Error (MAE) and the Root Mean Square Error (RMSE) metrics quantify the performance of the reference model and PFSIR-PR algorithm in regard to the states for which there is available quantitative information; i.e. cumulative leachate outflow and leachate discharge rate. It is

widely known that MAE and RMSE reveal the variability between individual estimates and observations, where MAEs and RMSEs closest to zero illustrate the best agreement with observations. These metrics are commonly expressed as follows:

$$\text{MAE} = \left|\bar{x}_t^i - y_t\right| \quad (49)$$

$$\text{RMSE} = \sqrt{\frac{1}{n} \cdot \sum_{t=1}^{N} \left(\bar{x}_t^i - y_t\right)^2} \quad (50)$$

Where $\bar{x}_t^i$ and y_t represent the mean particle values of the state vector and the measured data set at time t, respectively.

4.1.1 Cumulative Leachate Outflow

Table 4.3 summarizes the results in regard to the cumulative leachate outflow state. At first sight, it is apparent that the best compromise amongst the measured and the simulated cumulative leachate outflow is obtained with the PFSIR-PR by using daily DA events and $N = 100$ particles.

Table 4.3: Overview of results related to the cumulative leachate outflow state.

Case	State	Figure	MAE	RMSE
1	q_{cum}	4.1.a	27.35 m^3	35.75 m^3
2	q_{cum}	4.1.b	54.40 m^3	72.90 m^3
3	q_{cum}	4.1.c	23.10 m^3	30.38 m^3
4	q_{cum}	4.1.d	57.02 m^3	74.20 m^3
5	q_{cum}	4.1.a-d	2325.9 m^3	2970.32 m^3

In this instance; i.e. Case 3 from Table 4.3, the measured and the data-assimilated values are nearly similar, which can only be observed by having a closer look at Fig. 4.1.c. Further, the MAEs and RMSEs using daily DA time steps and $N = 100$ particles converge to much better values compared to the estimates obtained with the rest case scenarios; i.e. Case 1, 2 and 4 from Table 4.3.

According to the MAEs and RMSEs from Table 4.3; i.e. Cases 1 to 4, the number of particles does not seem to have a significant impact on the results. It is also evident that the PFSIR-PR approach using DA on a daily basis is slightly more effective than using DA every week on account of the fact that better MAEs and RMSEs are obtained. Taken as a whole, it turns out that when cumulative leachate outflow DA is performed the PFSIR-PR approach depends on the DA frequencies.

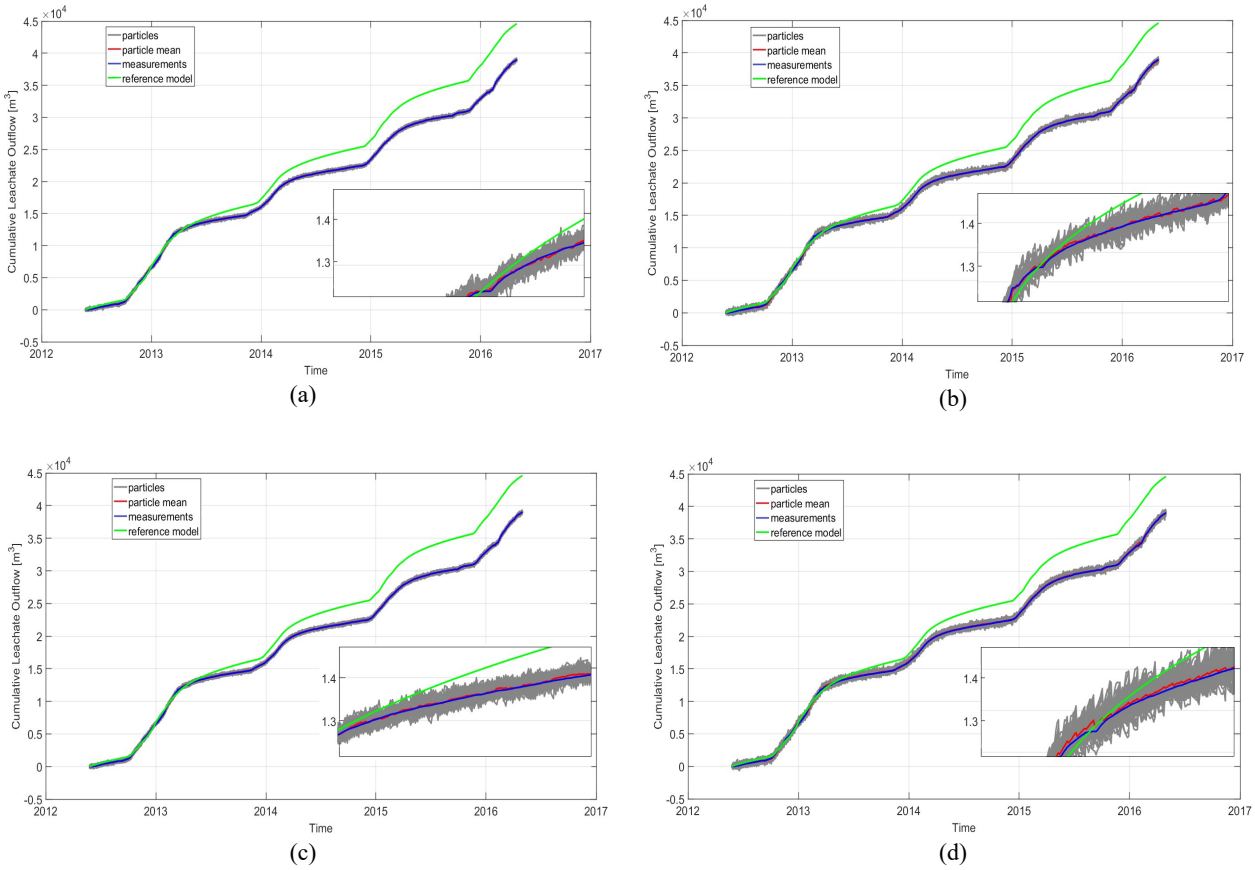

Fig. 4.1: Simulated and measured cumulative leachate outflow.

4.1.2 Leachate Discharge Rate

Table 4.4 reports the results related to the state of the leachate discharge rate. By and large, the PFSIR-PR method performs outstandingly well and is independent of the DA frequencies and particle numbers. In fact, Figs. 4.2.a-d verify that despite the use of different DA time steps and a diverse number of particles, the PFSIR-PR estimates are almost similar. Much relevant information can be obtained directly from the corresponding MAEs and RMSEs that are equivalent. Nevertheless, Fig. 4.2.b demonstrates that the most satisfactory reconciliation between the PFSIR-PR estimates and the measurements is obtained with the use of weekly leachate discharge rate DA events and $N = 50$ particles. This conclusion is made more precise by looking at the analogous MAEs and RMSEs.

Table 4.4: Overview of results related to the leachate discharge rate state.

Case	State	Figure	MAE	RMSE
1	$q_{discharge}$	4.2.a	9.07 m^3	0.37 m^3
2	$q_{discharge}$	4.2.b	9.00 m^3	0.11 m^3
3	$q_{discharge}$	4.2.c	9.81 m^3	3.31 m^3
4	$q_{discharge}$	4.2.d	10.1 m^3	4.13 m^3
5	$q_{discharge}$	4.2.a-d	9.27 m^3	3.92 m^3

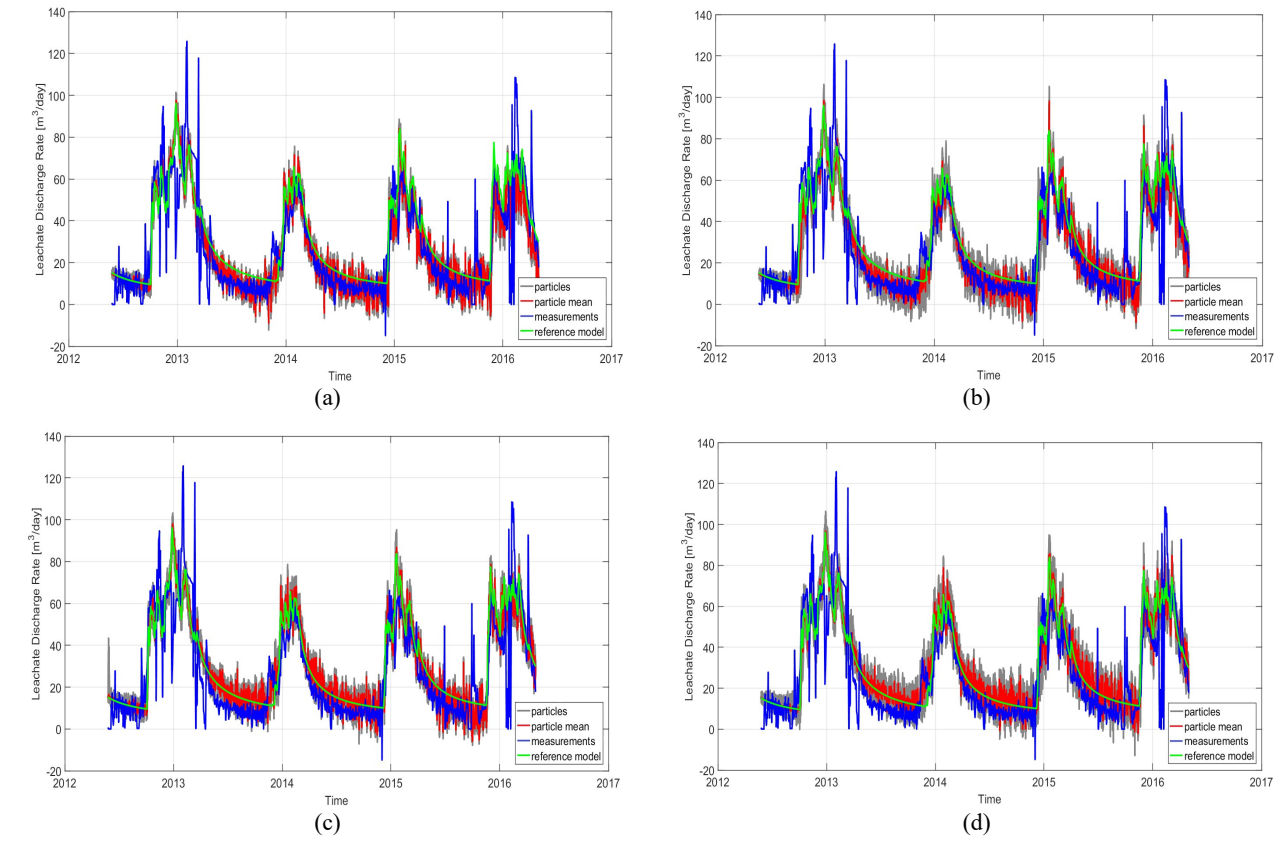

Fig. 4.2: Simulated and measured leachate discharge rate.

4.1.3 Cover Layer Water Content

The results with respect to the volumetric water content in the cover layer are listed in Table 4.5. The important point to note here is that the estimates provided by the reference model and the PFSIR-PR method using different DA frequencies and various particle numbers are quite the same, as Figs. 4.3.a-d illustrate. Furthermore, it can be seen that the particles are not overly dispersed. A more sophisticated view of this issue suggests that the particles arrive at a solution, and therefore, the PFSIR-PR forecasts can be viewed fairly reliable.

Table 4.5: Overview of results related to the cover layer water content state.

Case	State	Figure
1	θ	4.3.a
2	θ	4.3.b
3	θ	4.3.c
4	θ	4.3.d
5	θ	4.3.a-d

In addition, these figures indicate that the water content in the cover layer is periodically varying, increasing and decreasing during cold and warm periods, respectively. Of course, this assumption is plainly reinforced in view of the fact that although the water is evenly distributed into the landfill surface layer over

time (see Fig. 2.3), the potential evaporation throughout the summer months is remarkably high, which actually means that the cover layer water content is reduced during the summertime (see Fig. 2.4).

Another key thing to emphasize is that the PFSIR-PR estimates are independent of the DA frequencies and particle numbers. On the whole, it can be deduced that a high amount of water enters the waste body throughout the cold periods compared to the warm periods, as Figs. 4.3.a-b. show.

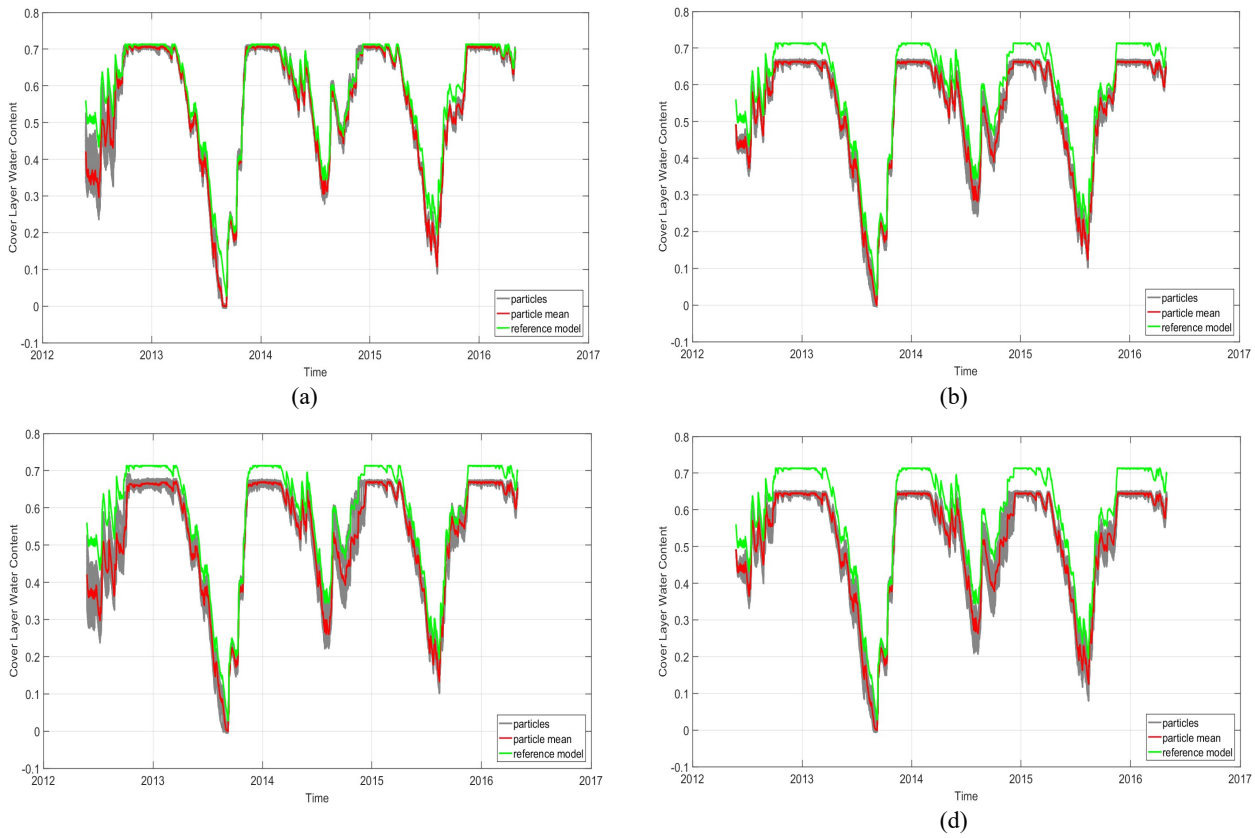

Fig. 4.3: Simulated and measured cover layer water content.

4.1.4 Water Infiltration

The findings apropos of the water infiltration state are illustrated in Table 4.6. In this regards, Figs. 4.5.a-b offer overwhelming evidence that the reference model underpredicts the amount of water that goes into the waste body.

Table 4.6: Overview of results related to the water infiltration state.

Case	State	Figure
1	Q_{inf}	4.4.a - 4.5.a
2	Q_{inf}	4.4.b - 4.5.b
3	Q_{inf}	4.4.c - 4.5.c
4	Q_{inf}	4.4.d - 4.5.d
5	Q_{inf}	4.4.a-d - 4.5.a-d

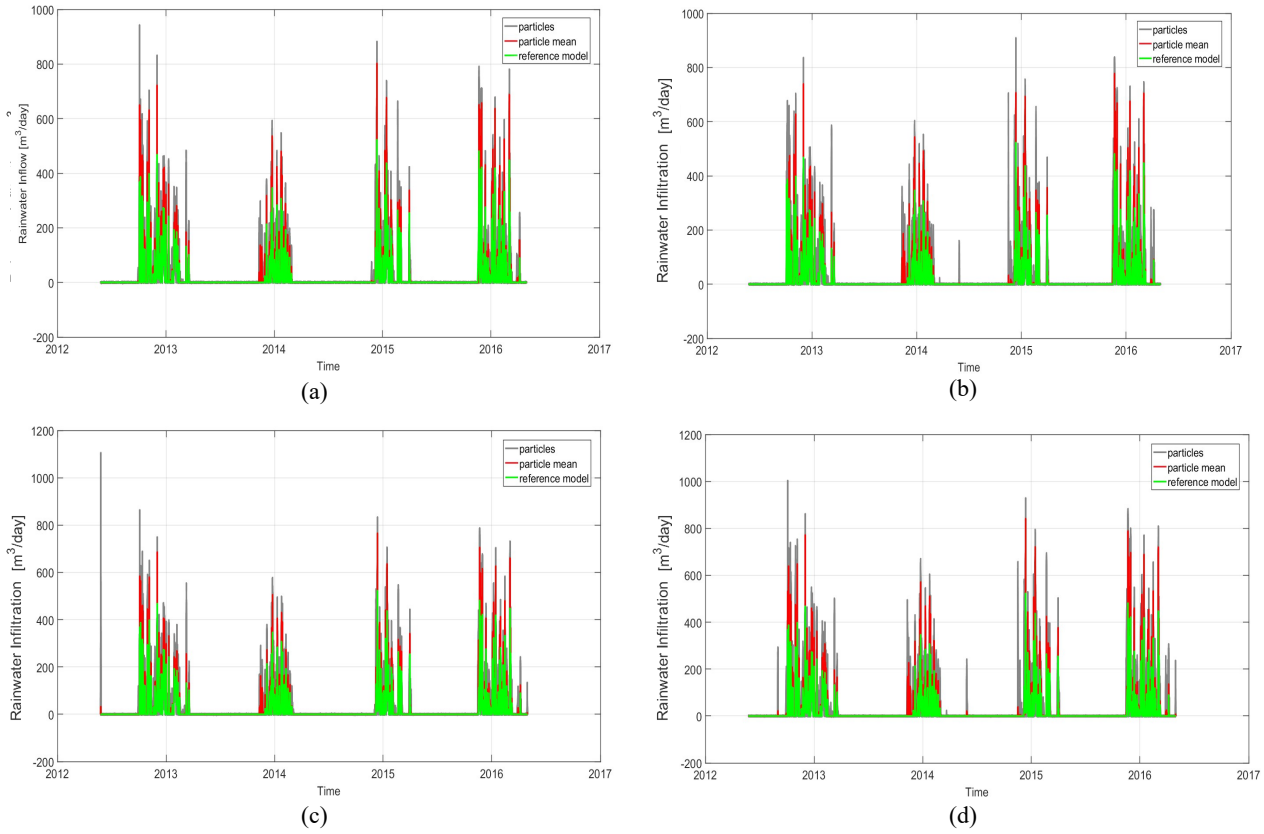

Fig. 4.4: Simulated and measured water infiltration.

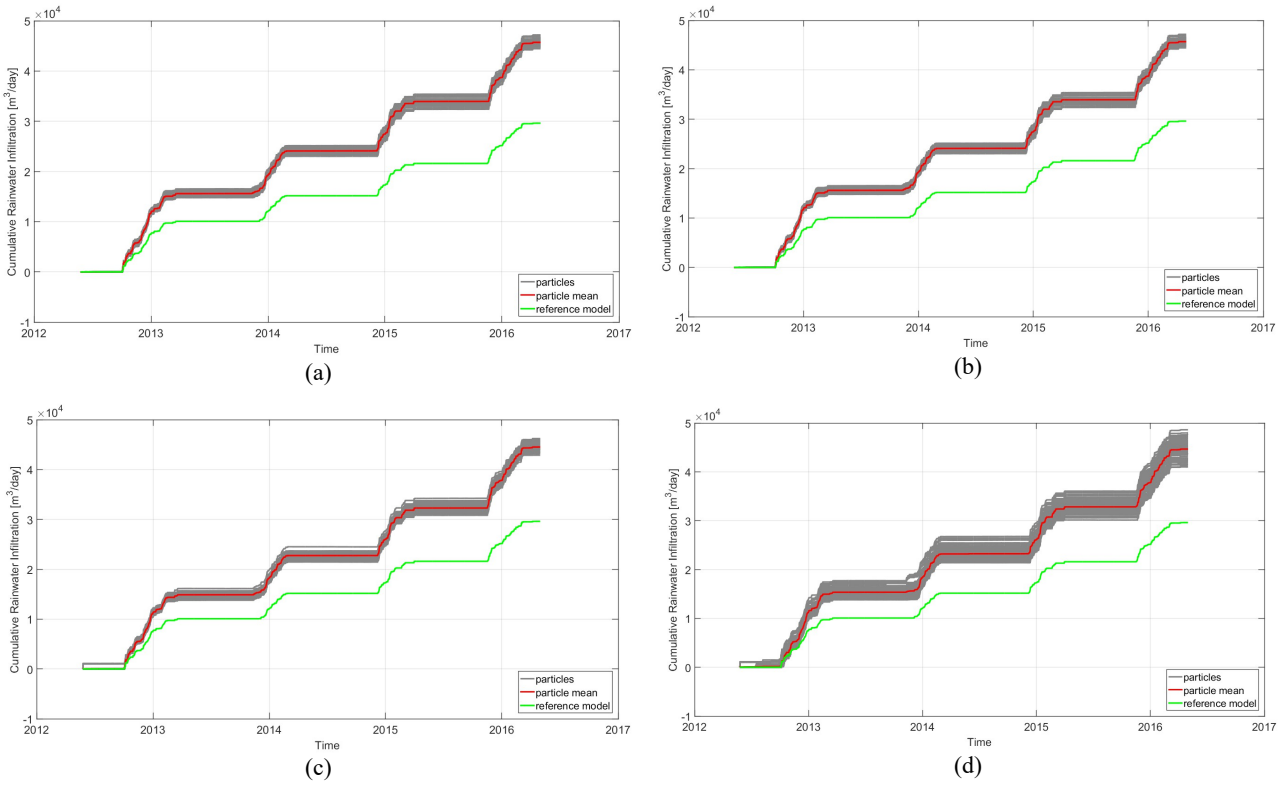

Fig. 4.5: Simulated and measured cumulative water infiltration.

On the contrary, the water infiltration estimates obtained with the PFSIR-PR approach seem to be higher. Another key thing to emphasize is that the PFSIR-PR estimates are independent of the DA frequences and particle numbers.

On the whole, it can be deduced that a high amount of water enters the waste body throughout the cold periods compared to the warm periods as shown in Figs. 4.4.a-d.

4.1.5 Waste Body Water Volume

Table 4.7 reports the findings as concerns the waste body water volume. By observing Figs. 4.6.a-d, one sees immediately that the estimates are incontrovertibly dissimilar by using sparse and dense observations with a different number of particles.

In the first place, Fig. 4.6.a reveals that through the use of $N = 50$ particles and daily DA time steps, the PFSIR-PR estimates of the waste body water content steadily increase over time. Secondly, Fig. 4.6.b evidently indicates that the water quantity in the waste body simulated with the PFSIR-PR approach is periodically varying by making use of $N = 50$ particles and weekly DA events. Note the considerable dispersion of particles as well as the fact that some of them have negative values as shown in Fig. 4.6.b. This indicates that huge uncertainty is associated with these estimates. Lastly, Figs. 4.6.c and 4.6.d illustrate that regardless of the DA frequencies, the water in the waste body is tremendously decreasing when it is estimated with the PFSIR-PR method using $N = 100$ particles.

The preceding observations when looked at from a closer point of view lead to several noteworthy conclusions. Initially, it can be argued that the most realistic estimates are represented by the cyclical variations of the waste body water volume. Logically thinking, it might be expected that the quantity of the immobile water in the waste body is rising when high amounts of water enter there; e.g. in the cold periods. By contrast, inconsiderable water infiltration into the waste body may result in a steady reduction of the motionless water; e.g. in the warm periods. In general, the afore-described process undoubtedly denotes a periodical fluctuation of the unmovable water in the waste body.

Table 4.7: Overview of results related to the waste body water volume state.

Case	State	Figure
1	V_{IM}	4.6.a
2	V_{IM}	4.6.b
3	V_{IM}	4.6.c
4	V_{IM}	4.6.d
5	V_{IM}	4.6.a-d

However, one more case merits mentioning here. In this regards, one may conjecture that the presence of specific heavy wastes in the waste body might prevent the water from flowing out of there, and consequently, the water is steadily increasing inside the main landfill body. Therefore, the assumption that the motionless water volume rises over time might be acceptable as well.

Quite the reverse, the findings indicating that the waste body water volume decreases over time do not manifest reasonableness. In fact, the estimated leachate discharge and water infiltration rates suggest (compare Figs 4.2.a-d with 4.4.a-d and 4.5.a-d) that higher amounts of water enter the landfill and less contaminated water (i.e. leachate) flows out from there.

The apparent lack of correlation between the PFSIR-PR estimates of the waste body water volume can be attributed to several factors. The prime cause of the discrepancy might be due to the use of different DA frequencies and particle numbers that result in different initial conditions (i.e. different initial state and parameter values). Also, it cannot be ruled out that unintended bias may result from inconsistent Gaussian noise values. Another possible rationalization for this is likely to be the inaccurate meteorological forcing data. A possible reason for this contradictory outcome might also be the effect of the perturbed parameters. On a wider level, a further experimental investigation is needed to determine the actual factors that result in the variations between the PFSIR-PR forecasts of this state variable.

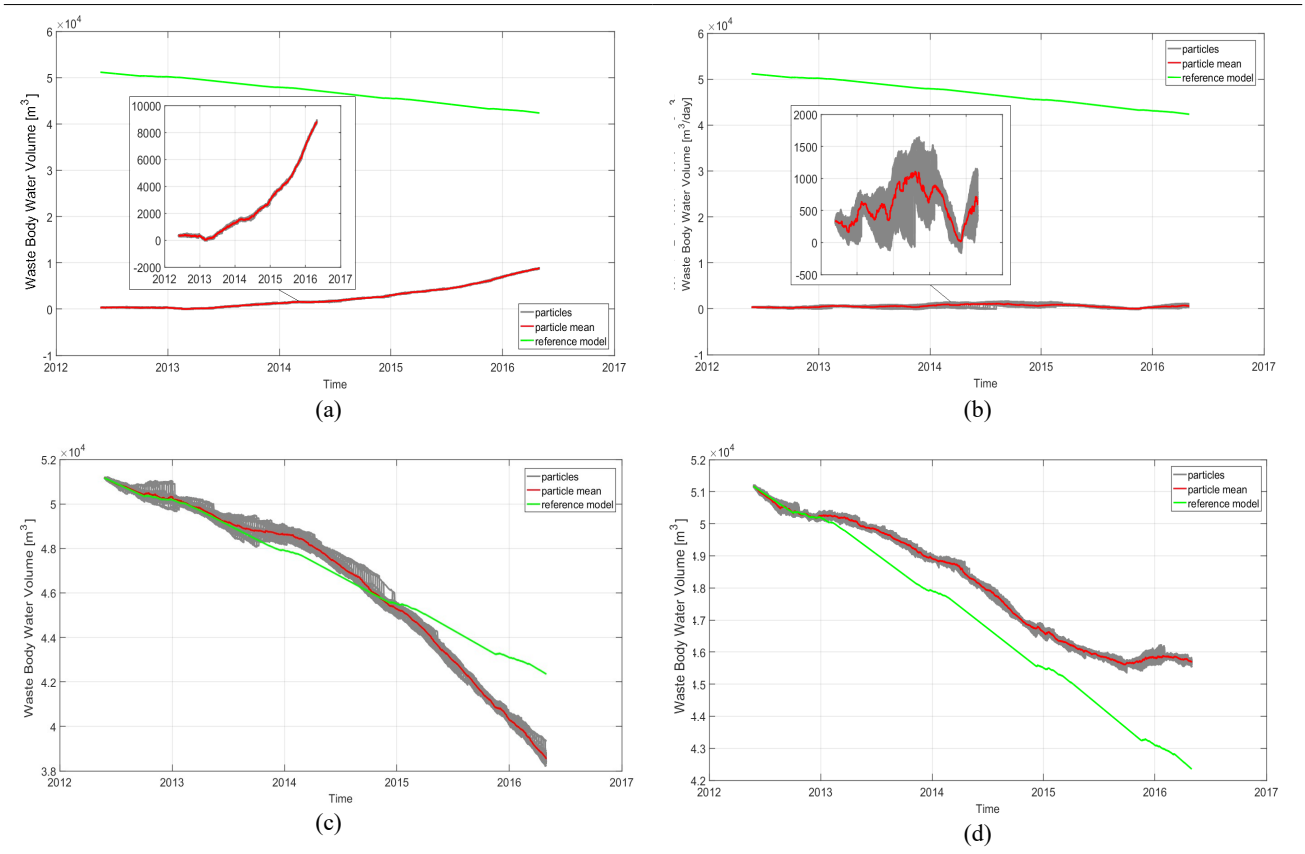

Fig. 4.6: Simulated and measured waste body water volume.

4.2. Assessement of Model Parameters

This section evaluates the PFSIR-PR derived parameter values. The mean values of the parameter particles obtained throughout the data assimilation process (i.e. from the beginning until the end of the simulations) are listed in Table 4.8. In the way indicated in section 3, the parameters are perturbed using equation (48) and are resampled by means of the PFSIR-PR approach. The coefficients α and δ in equation (48) are set to 0.99 and 0.975, respectively. In this manner, it is substantial to note that the water balance model operates assuming the parameters to be time-variant.

Two striking observations can be drawn from these findings. Fig. 4.7 reveals that the parameter histograms have the overall shape and size of a normal distribution, and additionally, Fig 4.8 shows that all the parameters seem to converge to a target value after 100 time steps.

Of equal importance, it can be asserted that by using different DA time steps and a various number of particles, some parameters converge to different values. Veritably, for each of the cases presented in Table 4.8, K_{sat}, m, μ_{fast}, and σ_{fast} center around diverse values. In contrast, the remaining parameters converge almost always to the same values.

Consequently, it is evident that changes in the DA frequency and in the number of particles impact remarkably upon K_{sat}, m, μ_{fast}, and σ_{fast}. In this context, the following section investigates in detail the effect of these parameters on the model outcome.

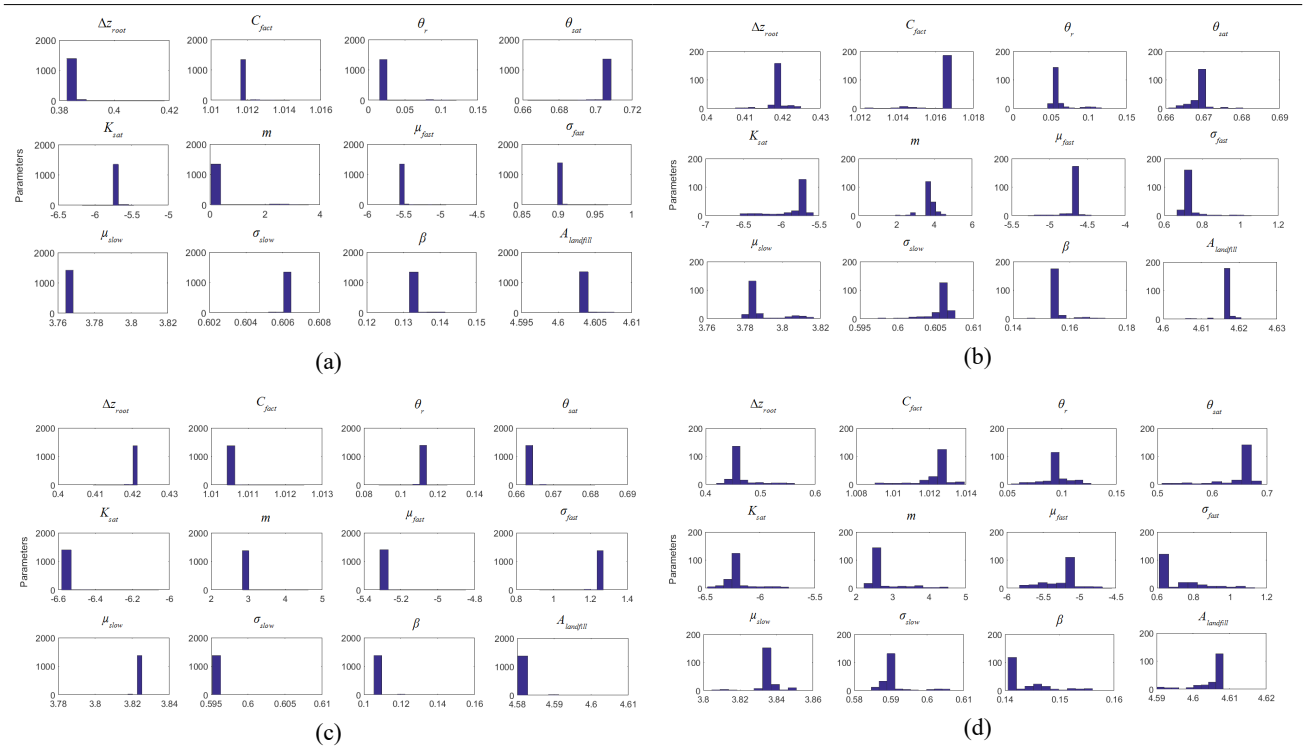

Fig. 4.7: Histogram of the mean values of the PFSIR-PR resampled parameter particles obtained as follows: (a) The PFSIR-PR approach is applied using daily data assimilation events and $N = 50$ particles, (b) The PFSIR-PR approach is applied using weekly data assimilation events and $N = 50$ particles, (c) The PFSIR-PR approach is applied using daily data assimilation events and $N = 100$ particles, (d) The PFSIR-PR approach is applied using weekly data assimilation events and $N = 100$ particles.

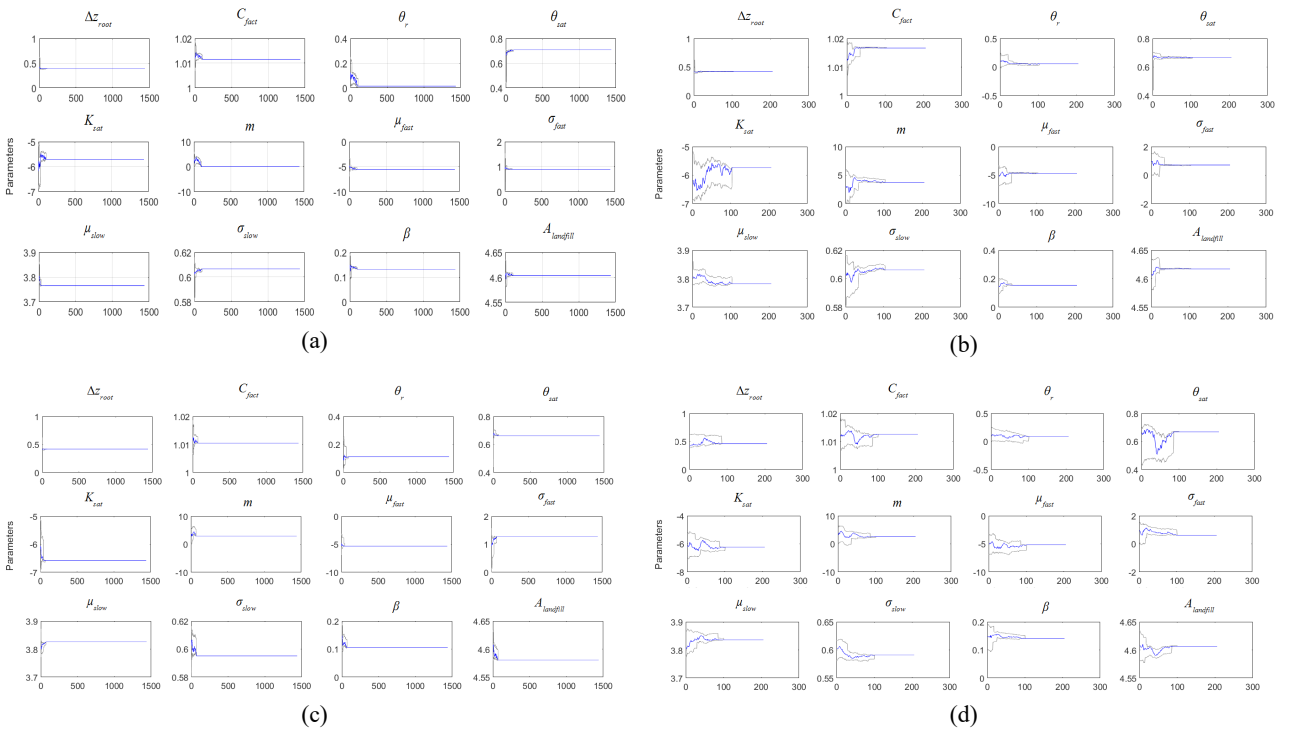

Fig. 4.8: Evolution of the parameter particles with PFSIR-PR using the following scenarios: (a) The PFSIR-PR approach is applied using daily data assimilation events and $N = 50$ particles, (b) The PFSIR-PR approach is applied using weekly data assimilation events and $N = 50$ particles, (c) The PFSIR-PR approach is applied using daily data assimilation events and $N = 100$ particles, (d) The PFSIR-PR approach is applied using weekly data assimilation events and $N = 100$ particles. In these plots, the blue line represents the mean values of the parameter particles and the gray lines illustrate the particle bounds (i.e. minimum and maximum values of parameter particles).

Table 4.8: Mean values of the parameter particles obtained with the PFSIR-PR approach.

Set†	Δz_{root} [m]	C_{fact} [-]	θ_r [-]	θ_{sat} [-]	K_{sat} [m/day]	m [-]	μ_{fast} [days]	σ_{fast} [days]	μ_{slow} [days]	σ_{slow} [days]	β [-]	$A_{landfill}$ [ha]
1	0.38	1.01	0.01	0.7	-5.69	0.18	-5.52	0.9	3.76	0.6	0.13	4.6
2	0.41	1.01	0.06	0.66	-5.84	3.72	-4.7	0.73	3.78	0.6	0.15	4.61
3	0.42	1.01	0.11	0.66	-6.56	3.04	-5.3	1.26	3.82	0.59	0.1	4.58
4	0.42	1.01	0.06	0.68	-5.79	2.59	-4.79	0.73	3.8	0.6	0.14	4.6

† Each parameter set listed in the table is obtained as follows:

Set 1: The PFSIR-PR approach is applied using daily data assimilation events and $N = 50$ particles.

Set 2: The PFSIR-PR approach is applied using weekly data assimilation events and $N = 50$ particles.

Set 3: The PFSIR-PR approach is applied using daily data assimilation events and $N = 100$ particles.

Set 4: The PFSIR-PR approach is applied using weekly data assimilation events and $N = 100$ particles.

4.3. Sensitivity analysis

The different waste body water volume estimates provided by the PFSIR-PR approach lead to many questions which require better examination. Overall, it is useful to identify what factors exert the most influence on the reference model and the PFSIR-PR method. Because of this, the current study conducts a sensitivity analysis taking into account a wide range of scenarios, such as:

1. Initially, the state and parameter sensitivity to the additive Gaussian noise is investigated. For this purpose, the PFSIR-PR method is performed by adding a smaller level of noise to the state variables. These noise values are generated by using the statistical properties listed in Table 4.9. Notice that it is not of interest to examine the impact of a larger noise level, because this can limit the representation of a real-case model error. Usually, Gaussian noise with zero mean and the standard deviation set to 1% - 15% of the state values is suggested (Marchetti et al. 2006; Moradkhani et al. 2012).

2. Following this, the impact of uncertain model parameters on the original model is explored in detail. In this environmental model, K_{sat}, m, μ_{fast}, and σ_{fast} should be certainly considered unreliable parameters. In reality, these parameters are not converged after the implementation of the DREAM algorithm (see Figs. 3.3 and 3.4), and additionally, they do not converge to certain values throughout the PFSIR-PR operation (see Table 4.8). To this end, the parameter sets presented in Table 4.8 are chosen to benchmark the performance of the water balance model without data assimilation. Of these parameter sets, it is obvious that K_{sat}, m, μ_{fast}, and σ_{fast} notably change whereas it can be posited that the other parameters are set to fixed values. This experimentation might go some way towards enhancing our understanding whether these uncertain parameters result in the inconsistency between model estimates and measurements.

3. In the same context, the initial mean values of the state particles (at time t_0) are compared with each other that have been obtained by using the initial values of the parameter particles (at time t_0), which, in turn, have been generated according to case scenarios 1 to 4 from Table 4.1. This is done in an effort to evaluate the effect of the width of the initial parameter distribution on the PFSIR-PR state estimates.

4. As to what is done next, it is tested whether the meteorological forcing data affects the performance of the PFSIR-PR approach. Drawing inspiration from the work of Plaza et al. (2012), this is done by disturbing the measured rainfall and potential evaporation data with an additive Gaussian noise, with zero mean and the standard deviation set to 1% of their values. In this case, noise is not added to the rainfall and potential evaporation data when a day without rain and potential evaporation is found. In this manner, the PFSIR-PR is performed by assuming that the model states, parameters, and inputs are all open to doubt.

5. Further analysis is also conducted with the sole aim of examining the effect of sparse observational data on the performance of the PFSIR-PR technique. In this scenario, the PFSIR-PR method is performed by choosing to use 2-weekly DA time steps. In summary, Table 4.10 details all the sensitivity analysis scenarios carried out in this research.

Turning now to the findings of this analysis, comprehensive results are obtained proving that the waste body water volume estimates are insensitive to different levels of noise (Scenarios 1 to 4 from Table 4.10). Actually, Fig. 4.9.e indicates that the estimates obtained using scenarios 1 to 4 are similar to the ones presented in Figs. 4.6.a-d. Regarding the other state variables, Figs. 4.9.a-d attest that the PFSIR-PR method performs fairly well using a lower level of noise. This claim is also substantiated by looking at the satisfactory MAEs and RMSEs of the measured states, as shown in Tables 4.11 and 4.12. As a last note, Fig. 4.9.f

provides irrefutable evidence that the parameters converge to some target values independently of changes in the state and noise values.

Table 4.9: Noise statistical properties selected to generate Gaussian random noises with respect to the state variables listed in the first column for the implementation of the PFSIR-PR method.

State	NMV†	NSDV‡	Unit
θ	0	0	-
q_{cum}	0	40	m^3
$q_{discharge}$	0	0.5	m^3/day
Q_{inf}	0	0.5	m^3/day
V_{IM}	0	5	m^3
V_{M}	0	0.1	m^3

†NM is the noise mean.

‡NSD is the noise standard deviation.

Table 4.10: Sensitivity analysis scenarios†.

Scenario 1	The PFSIR-PR approach is performed using daily DA events and N = 50 particles, while Gaussian noise generated according to the statistical properties listed in Table 4.9 is introduced to the state variables.
Scenario 2	The PFSIR-PR approach is performed using weekly DA events and N = 50 particles, while Gaussian noise generated according to the statistical properties listed in Table 4.9 is introduced to the state variables.
Scenario 3	The PFSIR-PR approach is performed using daily DA events and N = 100 particles, while Gaussian noise generated according to the statistical properties listed in Table 4.9 is introduced to the state variables.
Scenario 4	The PFSIR-PR approach is performed using weekly DA events and N = 100 particles, while Gaussian noise generated according to the statistical properties listed in Table 4.9 is introduced to the state variables.
Scenario 5	The reference model is run without DA using the parameter set 1 from Table 4.8.
Scenario 6	The reference model is run without DA using the parameter set 2 from Table 4.8.
Scenario 7	The reference model is run without DA using the parameter set 3 from Table 4.8.
Scenario 8	The reference model is run without DA using the parameter set 4 from Table 4.8.
Scenario 9	The PFSIR-PR approach is performed using the initial values of the parameter particles that are generated by using case scenarios 1 to 4 from Table 4.1.
Scenario 10	The PFSIR-PR approach is performed using daily DA events and N = 50 particles, while Gaussian noise is introduced to the model meteorological forcings with zero mean and the standard deviation set to 1% of their values.
Scenario 11	The PFSIR-PR approach is performed using 2-weekly DA events and N = 50 particles, while Gaussian noise generated according to the statistical properties listed in Table 4.2 is introduced to the state variables.
Scenario 12	The PFSIR-PR approach is performed using 2-weekly DA events and N = 100 particles, while Gaussian noise generated according to the statistical properties listed in Table 4.2 is introduced to the state variables.

†The simulated states and parameters with the PFSIR-PR approach are illustrated in the figures as the mean of their particles.

On the other hand, by making use of the parameter sets given in Table 4.8, the water balance model yields similar state estimates as Figs. 4.10.a-f illustrate (Scenarios 5 to 8 from Table 4.10). However, the MAEs and RMSEs in Tables 4.13 and 4.14 show that the bias still remains in the estimates when using the reference model without data assimilation. As a consequence, these findings point to the fact that the parameters K_{sat}, m, μ_{fast}, and σ_{fast} neither imrove nor further worsen the model estimates.

On another note, the findings in Table 4.17 (related to Scenario 9 from Table 4.10) indicate that the width of the initial distribution of the parameter particles is slightly different when using different number of particles (N = 50 and N = 100). However, it seems that even such marginally different initial parameter samples yield different initial state particles (check Tables 4.15 and 4.16). Obviously, different initial state particles lead to different state particles over time. This also explains the discrepancy between the waste body volume predictions as previously shown in Figs. 4.6.a-d.

Considering Figs. 4.11.a-e, one can deduce the considerable effect of the meteorological forcing data on the model simulations. In fact, it can be seen that the model states; e.g. particularly the leachate discharge rate and the cover layer water content, are adversely influenced by using different input data sets that is achieved by perturbing the original input data set at each time step (Scenario 10 from Table 4.10). Another clue to this claim lies in the rise of the MAEs and RMSEs as shown in Table 4.18, in comparison to the corresponding MAEs and RMSEs presented in Tables 4.3 and 4.4. However, surprisingly enough, Fig. 4.10.f indicates that the parameters are uninfluenced from the varying model inputs and reach convergence.

Last but not the least significant, it seems that the PFSIR-PR approach does not significantly suffer from problems of data scarcity. In truth, the findings in Figs. 4.12.a-e and the MAE and RMSE values in Tables 4.19 and 4.20 illustrate the satisfactory performance of the PFSIR-PR approach in the absence of large data set. On the other hand, Fig. 4.12.f illustrates that by using sparse data set and N = 50 particles the PFSIR-PR method does not result in the convergence of the model parameters; i.e. only K_{sat}, m, and μ_{slow} converge. In contrast, all the parameters are prone to reach convergence by using a larger number of particles; i.e. N = 100 particles.

Table 4.11: Sensitivity analysis results using scenarios 1 to 4 from Table 4.10 that relate to the cumulative leachate outflow state.

Case	State	Figure	MAE	RMSE
1	q_{cum}	4.9.a	47.04 m^3	70.42 m^3
2	q_{cum}	4.9.a	68.08 m^3	100.12 m^3
3	q_{cum}	4.9.a	39.89 m^3	51.98 m^3
4	q_{cum}	4.9.a	91.49 m^3	111.35 m^3

Table 4.12: Sensitivity analysis results using scenarios 1 to 4 from Table 4.10 that relate to the leachate discharge rate state.

Case	State	Figure	MAE	RMSE
1	$q_{discharge}$	4.9.b	9.31 m^3/day	3.34 m^3/day
2	$q_{discharge}$	4.9.b	8.58 m^3/day	0.03 m^3/day
3	$q_{discharge}$	4.9.b	9.78 m^3/day	3.73 m^3/day
4	$q_{discharge}$	4.9.b	9.68 m^3/day	3.5 m^3/day

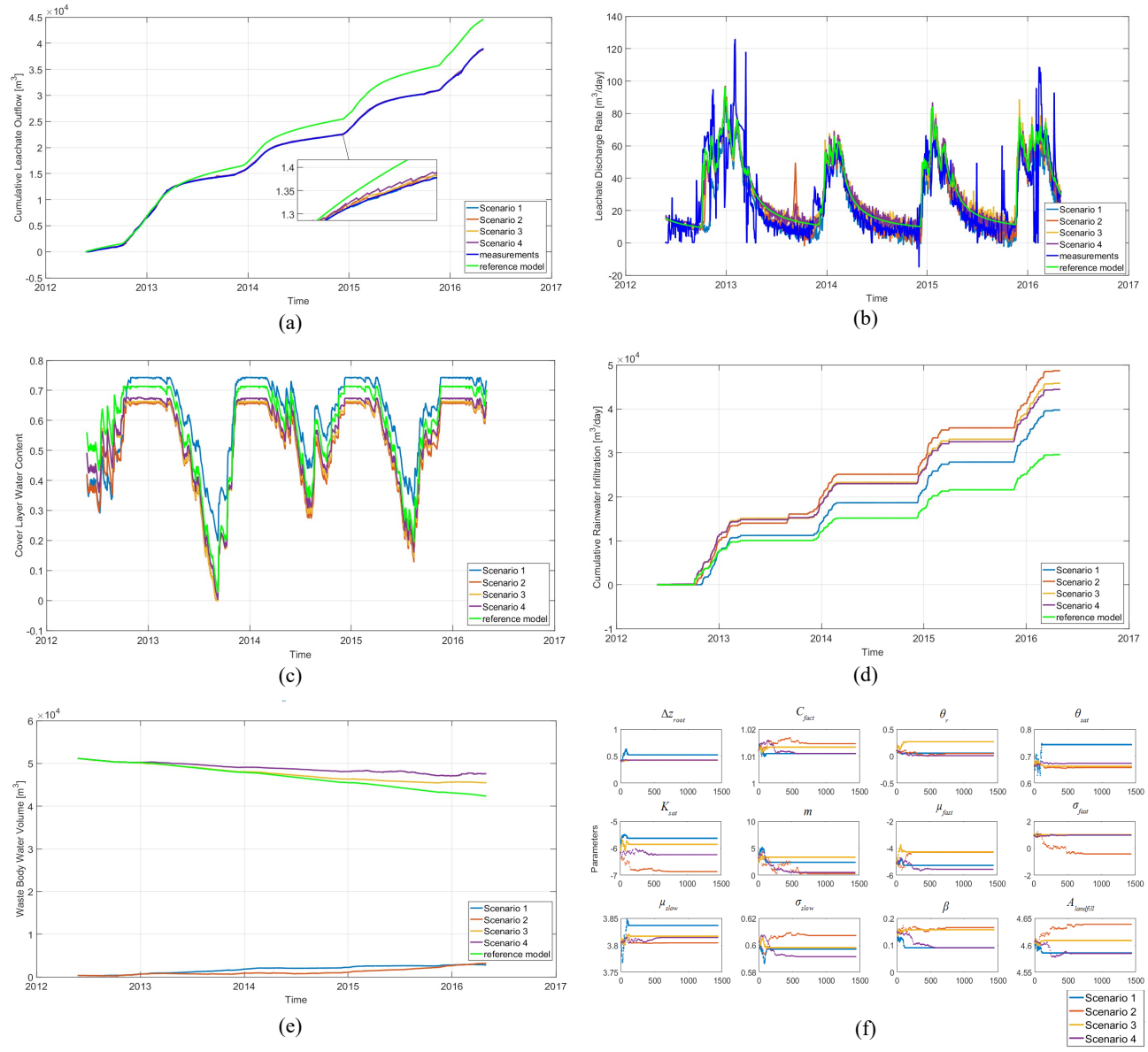

Fig. 4.9: Estimated states and parameters using scenarios 1 to 4 from Table 4.10: (a) Cumulative leachate outflow, (b) Leachate discharge rate, (c) Cover layer water content, (d) Cumulative water infiltration, (e) Waste body water volume, (f) Evolution of the mean values of the parameter particles obtained with PFSIR-PR.

Table 4.13: Sensitivity analysis results using scenarios 5 to 8 from Table 4.10 that relate to the cumulative leachate outflow state.

Case	State	Figure	MAE	RMSE
1	q_{cum}	4.10.a	$8.7 \cdot 10^3$ m^3	$1.07 \cdot 10^4$ m^3
2	q_{cum}	4.10.a	$8.64 \cdot 10^3$ m^3	$1.067 \cdot 10^4$ m^3
3	q_{cum}	4.10.a	$8.64 \cdot 10^3$ m^3	$1.066 \cdot 10^4$ m^3
4	q_{cum}	4.10.a	$8.61 \cdot 10^3$ m^3	$1.063 \cdot 10^4$ m^3

Table 4.14: Sensitivity analysis results using scenarios 5 to 8 from Table 4.10 that relate to the leachate discharge rate state.

Case	State	Figure	MAE	RMSE
1	$q_{discharge}$	4.10.b	20.86 m^3/day	4.48 m^3/day
2	$q_{discharge}$	4.10.b	20.71 m^3/day	4 m^3/day
3	$q_{discharge}$	4.10.b	20.66 m^3/day	3.85 m^3/day
4	$q_{discharge}$	4.10.b	20.61 m^3/day	3.68 m^3/day

Table 4.15: Mean values of the state variables simulated by the water balance model using case scenarios 1 and 2 from Table 4.1[†].

Values	States				
	q_{cum}	$q_{discharge}$	θ	Q_{inf}	V_{IM}
mean	0 m^3	14.7 m^3/day	0.42	0.11 m^3/day	332.90 m^3

[†]The findigs in this table are related to scenario 9 from Table 4.10.

Table 4.16: Mean values of the state variables simulated by the water balance model using case scenarios 3 and 4 from Table 4.1[†].

Values	States				
	q_{cum}	$q_{discharge}$	θ	Q_{inf}	V_{IM}
mean	0 m^3	15.28 m^3/day	0.49	0.0037 m^3/day	51169.49 m^3

[†]The findigs in this table are related to scenario 9 from Table 4.10.

Table 4.17: Minimum and maximum values of the parameter particles obtained with the PFSIR-PR approach using case scenarios 1 to 4 from Table 4.1[†].

Case	Values	Parameters											
		Δz_{root}	C_{fact}	θ_r	θ_{sat}	K_{sat}	m	μ_{fast}	σ_{fast}	μ_{slow}	σ_{slow}	β	$A_{landfill}$
		[m]	[-]	[-]	[-]	[m/day]	[-]	[days]	[days]	[days]	[days]	[-]	[ha]
1 & 2	minimum	0.38	1	$12 \cdot 10^{-3}$	0.43	-6.99	$7 \cdot 10^{-3}$	-6.87	$5 \cdot 10^{-3}$	3.77	0.58	$9 \cdot 10^{-3}$	4.58
	maximum	0.62	1.01	0.24	0.69	-4.86	5.95	-3.02	1.53	3.86	0.61	0.19	4.63
3 & 4	minimum	0.39	1	$21 \cdot 10^{-3}$	0.43	-6.99	$1 \cdot 10^{-2}$	-6.87	$5 \cdot 10^{-3}$	3.77	0.58	$9 \cdot 10^{-3}$	4.58
	maximum	0.62	1.01	0.24	0.69	-5.16	5.95	-3.27	1.53	3.86	0.61	0.19	4.63

[†]The findigs in this table are related to scenario 9 from Table 4.10.

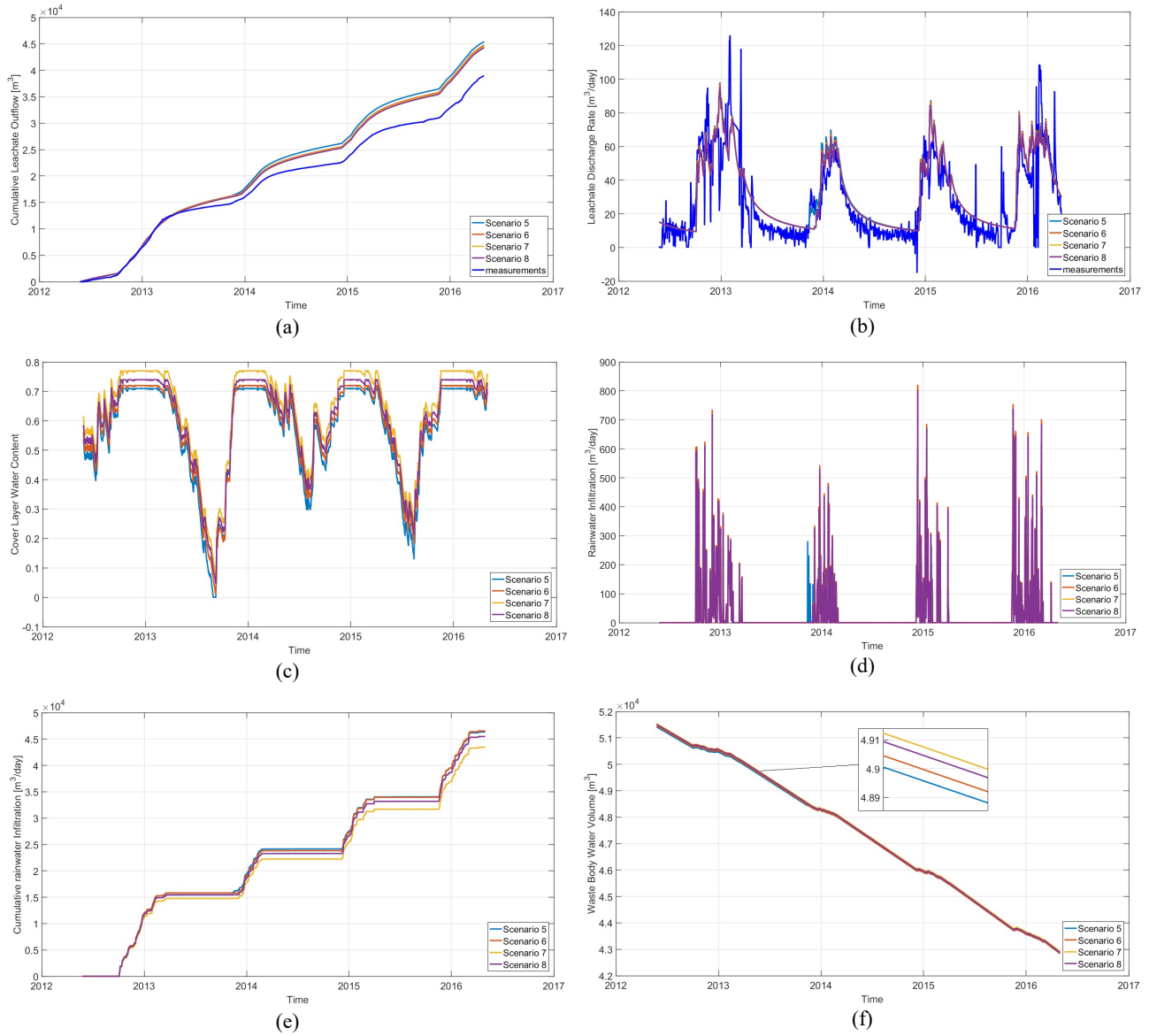

Fig. 4.10: Estimated states and parameters using scenarios 5 to 8 from Table 4.10: (a) Cumulative leachate outflow, (b) Leachate discharge rate, (c) Cover layer water content, (d) Water infiltration, (e) Cumulative water infiltration, (f) Waste body water volume.

Table 4.18: Sensitivity analysis results using scenario 10 from Table 4.10 that relate to the cumulative leachate outflow and leachate discharge states.

State	Figure	MAE	RMSE
q_{cum}	4.11.a	42.43 m^3	52.27 m^3
$q_{discharge}$	4.11.b	19.42 m^3/day	14.27 m^3/day

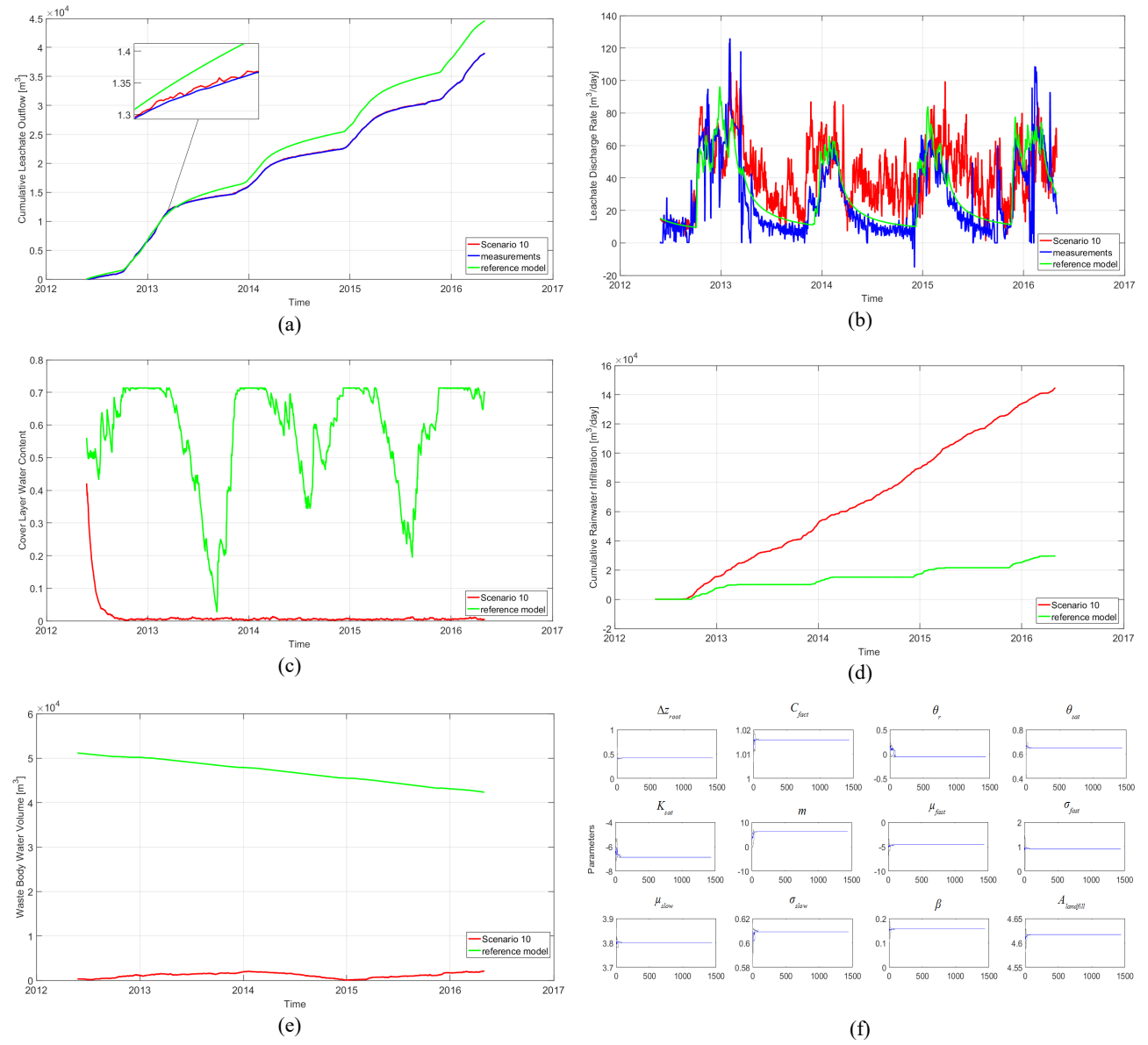

Fig. 4.11: Estimated states and parameters using scenario 10 from Table 4.10: (a) Cumulative leachate outflow, (b) Leachate discharge rate, (c) Cover layer water content, (d) Cumulative water infiltration, (e) Waste body water volume, (f) Evolution of the mean values of the parameter particles obtained with PFSIR-PR. In Fig.4.9.f, the blue line represents the mean values of the parameter particles and the gray lines illustrate the particle bounds (i.e. minimum and maximum values of parameter particles).

Table 4.19: Sensitivity analysis results using scenario 11 from Table 4.10 that relate to the cumulative leachate outflow and leachate discharge states.

State	Figure	MAE	RMSE
q_{cum}	4.12.a	76 m^3	113.3 m^3
$q_{discharge}$	4.12.b	9.27 m^3/day	0.82 m^3/day

Table 4.20: Sensitivity analysis results using scenario 12 from Table 4.10 that relate to the cumulative leachate outflow and leachate discharge states.

State	Figure	MAE	RMSE
q_{cum}	4.12.a	83.18 m^3	111.18 m^3
$q_{discharge}$	4.12.b	10.03 m^3/day	4.58 m^3/day

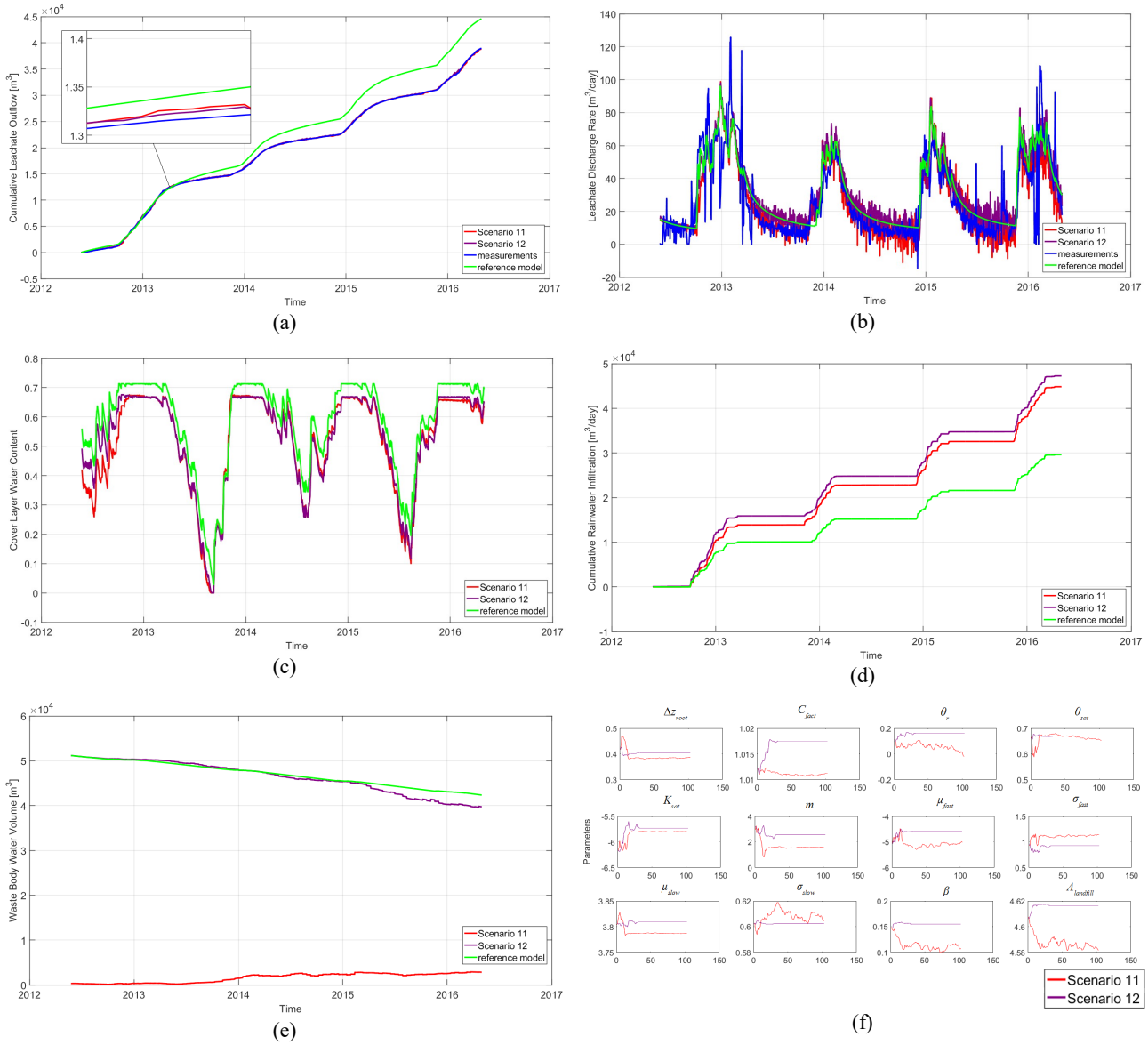

Fig. 4.12: Estimated states and parameters using scenarios 11 and 12 from Table 4.10: (a) Cumulative leachate outflow, (b) Leachate discharge rate, (c) Cover layer water content, (d) Cumulative water infiltration, (e) Waste body water volume, (f) Evolution of the mean values of the parameter particles obtained with PFSIR-PR.

5 CONCLUSIONS

This research has devised a methodology using an existing Particle Filter algorithm; i.e. the PFSIR-PR filter, for resolving the uncertainty problem associated with the water balance model. In fact, the proposed bias-correction scheme has enormously contributed to enhancing the predictability of this environmental model.

First of all, the PFSIR-PR approach has improved the predictions made with the water balance model of the cumulative leachate outflow, leachate discharge rate, cover layer water content and water infiltration into the waste body. However, large uncertainty remains regarding the waste body water volume.

The main achievement of this research is the improvement of consistency between unobserved states, parameters, and the data assimilated state variable. This was achieved by resampling the unobserved state and parameter values along with the data-assimilated cumulative leachate outflow state.

Furthermore, the resampled parameters evolved over time as non-stationary, stochastic variables according to Liu-West's parameter perturbation approach. The versatility of this approach has given surety to avoid any extreme replication of their values, and additionally, has contributed to obtaining converged parameter values. Although, it was shown that K_{sat}, m, μ_{fast}, and σ_{fast} converge to dissimilar values by using various DA time steps and a different number of particles. This might also imply the uncertain time-variant character of these parameters.

In the same context, the PFSIR-PR estimates of the waste body water volume were quite different after using different DA frequencies and diverse particle numbers. For this reason, this study has conducted a sensitivity analysis that showed that different initial parameter particles yield different initial state particles, which, in turn, lead to different state particles over time. This was actually the reason behind the different waste body water volume estimates obtained with the PFSIR-PR approach.

This sensitivity analysis has also revealed the insignificant interdependence between the model states and the aforementioned uncertain parameters when using the reference model without DA. From this analysis, it was also corroborated that the input data set; i.e. measured precipitation and potential evaporation data, has a significant impact on the PFSIR-PR method, and maybe on the original model as well. In this sensitivity inquiry, it has been also shown that the noise level does not play an important role in this particular filtering scheme.

The robustness of the PFSIR-PR filter has been also tested for different assimilation frequencies; i.e. from daily to 2-weekly DA assimilation time steps. In this regards, the scarcity of data has not induced any noteworthy effects on the performance of this data assimilation technique as concerns the state variables. However, in this testing, the parameters do not reach converge when little data is available and a small number of particles are used. On the contrary, by making use of a large number of particles the PFSIR-PR efficiently guarantees the parameter convergence. This conclusion points to the fact that the decrease of the number of

particles along with the reduction in the DA time steps results in loss of information and therefore negatively affects the filtering performance with regard to the model parameters.

In consideration of the foregoing, it can be deduced that the main uncertain sources of this prediction model are: a) the meteorological forcing data, and b) the afore-described uncertain model parameters; i.e. K_{sat}, m, μ_{fast}, and σ_{fast}. In view of this, an important issue to investigate for future studies is to further examine the influence of the input model data and the impact of the unreliable model parameters on the model outcome.

In this context, it would be beneficial to model a) the amount of water that infiltrates into the landfill and b) the amount of water that evaporates from the landfill surface layer. This might leads to obtain more realistic inputs to drive the model, and may also improve the model performance.

With regard to the uncertain parameters, it would be useful, but also challenging to conduct monthly or seasonal parameter estimation analysis in an attempt to detect typical monthly or seasonal patterns of dominant parameters linked to the processes that take place within the landfill environment at the same investigated periods.

Bibliography

1. C. Andrieu, A. Doucet, Singh S. S., and V. B. Tadic (2004), Particle Methods for Change Detection, System Identification and Control, *IEEE Trans. Signal Processing*, **92**(3): 423-438.
[Available online: http://dx.doi.org/10.1109/JPROC.2003.823142]

2. C. Andrieu, Doucet A., and R. Holenstein (2010), Particle Markov Chain Monte Carlo Methods, *Journal of the Royal Statistical Society*, **72**(3): 269-342.
[Available online: http://dx.doi.org/1369-7412/10/72269]

3. S. Arulampalam, S. Maskell, N. Gordon, and T. Clapp (2002), A Tutorial on Particle Filters for on-line Non-linear/Non-Gaussian Bayesian Tracking, *IEEE Trans. Signal Processing*, **50**(2): 174-188.
[Available online: http://dx.doi.org/10.1109/78.978374]

4. J. Carpenter, P. Clifford, and P. Fearnhead (1999), Improved particle filter for nonlinear problems, *Proc. Inst. Elect. Eng.*, *Radar*, *Sonar*, *Navig.*

5. C. M. Carvalho, M. S. Johannes, H. F. Lopes, and G. P. Nicholas (2010), Particle Learning and Smoothing, *Statistical Science Journal*, **25**(1): 88-106.
[Available online: http://dx.doi.org/10.1214/10-STS325]

6. S.-Y. Chang and S. M. I. Latif (2009), Use of Kalman Filter and Particle Filter in a One Dimensional Leachate Transport Model, *In Proceedings of the 2007 National Conference on Environmental Science and Technology*, 157-163.
[Available online: http://dx.doi.org/978-0-387-88483-7]

7. S.-Y Chang and X. Li (2009), Organic Pollutant Transport in Groundwater Using Particle Filter, *In Proceedings of the 2007 National Conference on Environmental Science and Technology*, 165-171.
[Available online: http://dx.doi.org/978-0-387-88483-7]

8. S.-Y. Chang, T. Chowhan, and S. Latif (2012), State and Parameter Estimation with a SIR Particle Filter in a Three-Dimensional Groundwater Pollutant Transport Model, *J. Environ. Eng.*, **138**(11): 1114-1121.
[Available online: http://dx.doi.org/10.1061/(ASCE)EE.1943-7870.0000584]

9. Z. Chen (2003), From Kalman Filters to Particle Filters, and Beyond, *Statistics*, **182**(1): 1-69.
[Available online: http://dx.doi.org/10.1080/02331880309257]

10. C. M. DeChant and H. Moradkhani (2012), Examining the effectiveness and robustness of sequential data assimilation methods for quantification of uncertainty in hydrologic forecasting, *Water Resources Research*, **48**(4).
[Available online: http://dx.doi.org/10.1029/2011WR011011]

11. A. Doucet, S. Godsill, and C. Andrieu (2000), On sequential Monte Carlo sampling methods for Bayesian filtering, *Statist. Comput.*, **10**(3): 197-208.
[Available online: http://dx.doi.org/10.1023/A:1008935410038]

12. A. Doucet, J. F. G. de Freitas, and N. J. Gordon (2001), Sequential Monte Carlo Methods in Practice, A. Doucet, J. F. G. de Freitas, and N. J. Gordon, Eds. New York: Springer-Verlag.

13. R. Douc, E. Moulines, and O. Cappé (2005), Comparison of Resampling Schemes for Particle Filtering, *In Proceedings of the 4th International Symposium on Image and Signal Processing and Analysis*, **I**: 64-69.
[Available online: https://arxiv.org/abs/cs/0507025]

14. Y. Erol, L. Li, B. Ramsundar, and S. J. Russell (2013), The Extended Parameter Filter, ICML (3), 1103-1111.
[Available online: https://arxiv.org/abs/1305.1704]

15. N. Gordon, D. Salmond, and A. F. M. Smith (1993), Novel approach to nonlinear and non-Gaussian Bayesian state estimation, *Proc. Inst. Elect. Eng.*, *F*, **140**: 7-113.

16. A. Gelman and D. B. Rubin (1992), Inference from iterative simulation using multiple sequences, *Statistical Science Journal*, **7**(4): 457-472.
[Available online: http://dx.doi.org/10.1214/ss2F1177011136]

17. T.J. Heimovaara, A. Bun, and A.G. van Turnhout (2015). Water balance modeling for estimation of residence time of water in a full scale landfill using a data-assimilation approach, HPM6: The 6th International Workshop Hydro-Physico-Mechanics of Landfills, Delft, The Netherlands.

18. J. D. Hol, T. B. Schön, and F. Gustafsson (2006), On Resampling Algorithms for Particle Filters, Division of Automatic Control, *IEEE Trans. Signal Processing.*
[Available online: http://dx.doi.org/10.1109/NSSPW.2006.4378824]

19. Y. Hu, P. Baraldi, F. Di Maio, and E. Zio (2015), A particle filtering and kernel smoothing-based approach for new design component prognostics, *Reliability Engineering and System Safety*, **134**: 19-31.
[Available online: http://dx.doi.org/10.1016/j.ress.2014.10.003]

20. Y. Hu, P. Baraldi, F. Di Maio, E. Zio (2016), A Prognostic Approach Based on Particle Filtering and Optimized Tuning Kernel Smoothing, *IEEE Trans. Reliability*, **65**(2): 718-735.
[Available online: http://dx.doi.org/10.1109/TR.2015.2500681]

20. A. Jin and S.-Y. Chang (2009), Radioactive Contaminanant Transport in Subsurface Porous Environment, *In Proceedings of the 2007 National Conference on Environmental Science and Technology*, 181-188.
[Available online: http://dx.doi.org/10.1007/978-0-387-88483-7_24]

21. W. Jury and K. Roth (1990), *Transfer Functions and Solute Movement through Soil; Theory and Applications*, Birkhäuser Verlag, Basel, Boston, Berlin.

22. L. A. Konstantaki, R. Ghose, and D. Draganov, T. J. Heimovaara, (2015), *A geophysical toolbox for imaging and characterization of a landfill*, HPM6: The 6th International Workshop Hydro-Physico-Mechanics of Landfills, Delft, The Netherlands.
[Available online: http://dx.doi.org/10.1190/geo2013-0099.1]

23. G. Kitagawa, Monte Carlo filter and smoother for non-Gaussian nonlinear state space models (1996), *J. Comput. Graph. Statist.*, **5**(1): 1-25.
[Available online: http://dx.doi.org/10.2307/1390750]

24. P. J. Van Leeuwen (2009), Particle filtering in geophysical systems, *Monthly Weather Review*, **137**(12): 4089-4114.
[Available online: http://dx.doi.org/10.1175/2009MWR2835.1]

25. P. J. Van Leeuwen (2010), Nonlinear data assimilation in geosciences: an extremely efficient particle filter, *Q. J. R. Meteoral. Soc.*, **136**(653): 1991-1999.
[Available online: http://dx.doi.org/10.1002/qj.699]

26. J. Liu and M. West (2001), Combined parameters and state estimation in simulationbased filtering, In *Sequential Monte Carlo Methods in Practice* (Eds. A. Doucet, N. de Freitas and N. Gordon), Springer-Verlag, New York.

27. Y. Liu and H. V. Gupta (2007), Uncertainty in hydrologic modeling: Toward an integrated data assimilation framework, *Water Resources Research*, **43**(7).
[Available online: http://dx.doi.org/10.1029/2006WR005756]

28. J. P. Mattern, M. Dowd, K. Fennel (2013), Particle filter-based data assimilation for a three-dimensional biological ocean model and satellite observations, *Journal of Geophysical Research*, **118**(5): 2746-2760.
[Available online: http://dx.doi.org/10.1002/jgrc.20213]

29. M. Van Meeteren, D. Timens, K. U. Heiyer (2009), Feasibility study sustainable emission reduction at the existing landfills Kragge and Wieringermeer in the Netherlands, Royal Haskoning.

30. L. Marchetti, G. Grisetti, L. Iocchi (2006), A Comparative Analysis of Particle Filter Based Localization Methods, *Lecture Notes in Computer Science*, **4434**: 442-449.
[Available online: http://dx.doi.org/10.1007/978-3-540-74024-7_44]

31. H. Moradkhani, S. Sorooshian, H. V. Gupta, and P. R. Houser (2005a), Dual state-parameter estimation of hydrological models using ensemble Kalman filter, *Advances in Water Resources*, **28**(2): 135-147.
[Available online: http://dx.doi.org/10.1016/j.advwatres.2004.09.002]

32. H. Moradkhani, K.-L. Hsu, H. V. Gupta, and S. Sorooshian (2005b), Uncertainty assessment of hydrologic model states and parameters: Sequential data assimilation using the particle filter, *Water Resources Research*, **41**(5).
[Available online: http://dx.doi.org/10.1029/2004WR003604]

33. H. Moradkhani, C. M. DeChant, and S. Sorooshian (2012), Evolution of ensemble data assimilation for uncertainty quantification using the particle filter-Markov chain Monte Carlo method, *Water Resources Research*, **48**(12).
[Available online: http://dx.doi.org/10.1029/2012WR012144]

34. S. Nakano, G. Ueno, and T. Higuchi (2007), Merging particle filter for sequential data assimilation. Nonlinear Processes in Geophysics, *Nonlin. Processes Geophys.*, **14**(4): 395-408.
[Available online: http://dx.doi.org/10.5194/npg-14-395-2007]

35. K. Nagarajan, J. Judge, W. D. Graham, and A. Monsivais-Huertero (2010), Particle Filter-based assimilation algorithms for improved estimation of root-zone soil moisture under dynamic vegetation conditions, *Advances in Water Resources*, **34**(4): 433-477.
[Available online: http://dx.doi.org/10.1016/j.advwatres.2010.09.019]

36. L. E. Olivier, B. Huang, and I. K. Craig (2007), Dual particle filters for state and parameter estimation with application to a run-ofmine ore mill, *Journal of Process Control*, **22**(4): 710-717.
[Available online: http://dx.doi.org/10.1016/j.jprocont.2012.02.009]

37. D. A. Plaza-Guingla, R. De Keyser, G. J. M. De Lannoy, L. Giustarini, P. Matgen, and V. R. N. Pauwels(2012), The importance of parameter resampling for soil moisture data assimilation into hydrologic models using the particle filter, *Hydrol. Earth Syst. Sci.*, **16**(2): 375-390.
[Available online]: http://dx.doi.org/10.5194/hess-16-375-2012

38. D. A. Plaza-Guingla, R. De Keyser, G. J. M. De Lannoy, L. Giustarini, P. Matgen, and V. R. N. Pauwels (2013), Improving particle filters in rainfall-runoff models: Application of the resample-move step and the ensemble Gaussian particle filter, *Water Resources Research*, **49**(7): 4005-4021.
[Available online: http://dx.doi.org/10.1002/wrcr.20291]

39. H. M. Regan, M. Colyvan, M. A. Burgman, (2002), A taxonomy and treatment of uncertainty for ecology and conservation biology, *Ecol. Appl*. **12**(2): 618-628.
[Available online: http://dx.doi.org/10.2307/3060967]

40. I. M. Rekleitis (2004), A particle filter tutorial for mobile robot localization. Technical Report TR-CIM-04-02, Centre for Intelligent Machines, McGill University, 34800 University St., Montreal, Québec, CANADA H3A 2A7.

41. J. Rings, J. A. Vrugt, G. Schoups, J. A. Huisman, and H. Vereecken (2012), Bayesian model averaging using particle filtering and Gaussian mixture modeling: Theory, concepts, and simulation experiments, *Water Resources Research*, **48**(5).
[Available online: http://dx.doi.org/10.1029/2011WR011607]

42. A. R. Robinson and P. F. J. Lermusiaux (2002), Data assimilation for modeling and predicting coupled physical-biological interactions in the sea, *The Sea*, **12**: 475-536.

43. N. H. Rosqvist and G. Destouni (2000), Solute transport through preferential pathways in municipal solid waste, *J. Contam. Hydrol*. **46**(1-2): 39-60.
[Available online: http://dx.doi.org/10.1016/S0169-7722(00)00127-3]

44. N. H. Rosqvist, L. H. Dollar, A. B. Fourie (2005), Preferential flow in municipal solid waste and implications for long-term leachate quality: valuation of laboratory-scale experiments. *Waste Manag. Res.,* **23**(4): 367-380.
[Available online: http://dx.doi.org/10.1177/0734242X05056995]

45. D. Russo, W. A. Jury, and G. L. Butters, (1989), Numerical analysis of solute transport during transient irrigation: 2. The effect of immobile water, *Water Resources Research*, **25**(10): 2119-2127.
[Available online: http://dx.doi.org/10.1029/WR025i010p02119]

46. G. Schoups and J. A.Vrugt (2010), A formal likelihood function for parameter and predictive inference of hydrologic models with correlated, heteroscedastic, and non-Gaussian errors, *Water Resources Research*, **46**(10).
[Available online: http://dx.doi.org/10.1029/2009WR008933]

47. S. Thrun (2002), Particle filters in robotics, *In Proceedings of the 17th Annual Conference on Uncertainty in AI (UAI*), 511-518.

48. L. Uusitalo, A. Lehikoinen, I. Helle, K. Myrberg (2015), An overview of methods to evaluate uncertainty of deterministic models in decision support, *Environmental Modelling & Software*, **63**: 24-31.
[Available online: http://dx.doi.org/10.1016/j.envsoft.2014.09.017]

49. J. A. Vrugt, H. V. Gupta, W. Bouten, and S. Sorooshian (2003), A shuffled complex evolution Metropolis algorithm for optimization and uncertainty assessment of hydrologic model parameters, *Water Resources Research*, **39**(8).
[Available online: http://doi.org/10.1029/2002WR001642]

50. J. A. Vrugt, C. G. H. Diks, H. V. Gupta, W. Bouten, and J. M. Verstraten (2005), Improved treatment of uncertainty in hydrologic modeling: Combining the strengths of global optimization and data assimilation, *Water Resources Research*, **41**(1): 1-17.
[Available online: http://doi.org/10.1029/2004WR003059]

51. J. A. Vrugt, H. V. Gupta, B. O. Nuallain, and W. Bouten (2006), Real-Time Data Assimilation for Operational Ensemble Streamflow Forecasting, *Journal of Hydrometeorology*, **7**(3): 548-565.
[Available online: http://doi.org/10.1175/JHM504.1]

52. J. A. Vrugt, C. J. F. ter Braak, H. V. Gupta, and B. A. Robinson (2008), A Equifinality of formal (DREAM) and informal (GLUE) Bayesian approaches in hydrologic modeling, *Stochastic Environmental Research and Risk Assessment*, **23**(7): 1011-1026.
[Available online: http://doi.org/10.1007/s00477-008-0274-y]

53. E. Laloy and J. A.Vrugt (2012), High-dimensional posterior exploration of hydrologic models using multiple-try DREAM (ZS) and high-performance computing, *Water Resources Research*, **48**(1).
[Available online: http://doi.org/10.1029/2011WR010608]

54. J. A. Vrugt, C. J. F. ter Braak, C. G. H. Diks, and G. Schoups (2013), Hydrologic data assimilation using particle Markov chain Monte Carlo simulation, *Advances in Water Resources Journal*, **51**: 457-478.
[Available online: http://doi.org/10.1016/j.advwatres.2012.04.002]

55. M. West (1993), Mixture models, Monte Carlo, Bayesian updating and dynamic models. *Comput Sci Statist*, **24**:325-333.

56. H. Yan and H. Moradkhani (2016), Combined assimilation of streamflow and satellite soil moisture with the particle filter and geostatistical modeling, *Advances in Water Resources*, **94**: 364-378.
[Available online: http://doi.org/10.1016/j.advwatres.2016.06.002]

57. A. Zacharof and A. Butler (2004a), Stochastic modelling of landfill processes incorporating waste heterogeneity and data uncertainty. *Waste Manag*. **24**(3): 241-250.
[Available online: http://dx.doi.org/10.1016/j.wasman.2003.12.001]

58. A. I. Zacharof and A. P. Butler (2004b), Stochastic modelling of landfill leachate and biogas production incorporating waste heterogeneity. Model formulation and uncertainty analysis. *Waste Manag*. **24**(5): 453-462.
[Available online: http://dx.doi.org/10.1016/j.wasman.2003.09.010]

APPENDIX A

In this appendix, the analytical derivation of equation (35) that describes the posterior probability of the state vector X~x_t is detailedly demonstrated. To start with, for the sake of convenience, Bayes' law equation is written in a time domain form, as follows:

$$p(x_t \mid y_t) = \frac{p(y_t \mid x_t) \cdot p(x_t)}{\int p(y_t \mid x_t) \cdot p(x_t) dx_t} \quad (51)$$

After that, the denominator of equation (51) is expressed as:

$$p(y_t \mid y_{t-1}) = \int p(y_t \mid x_t) \cdot p(x_t) dx_t \quad (52)$$

In what follows, the substitution of equation (33) into equation (51) leads to:

$$p(x_t \mid y_t) = \frac{p(y_t \mid x_t) \cdot \frac{1}{N} \cdot \sum_{i=1}^{N} \delta_{x_t^i} \cdot (x_t - x_t^i)}{p(y_t \mid y_{t-1})}$$

$$= \frac{\frac{1}{N} \cdot \sum_{i=1}^{N} p(y_t \mid x_t^i) \cdot \delta_{x_t^i} \cdot (x_t - x_t^i)}{p(y_t \mid y_{t-1})}$$

$$= \frac{\frac{1}{N} \cdot \sum_{i=1}^{N} w_t^i \cdot \delta_{x_t^i} \cdot (x_t - x_t^i)}{p(y_t \mid y_{t-1})} \quad (53)$$

It is also known that the denominator of equation (53) is defined as such:

$$p(y_t \mid y_{t-1}) = \frac{1}{N} \cdot \sum_{i=1}^{N} w_t^i \quad (54)$$

Finally, by inserting equation (54) into equation (53) the posterior probability obtains its final form:

$$p(x_t \mid y_{1:t}) = \sum_{i=1}^{N} w_t^i \cdot \delta_{x_t^i} \cdot (x_t - x_t^i) \quad (55)$$

Where equation (55) is plainly equivalent to equation (35).

APPENDIX B

Here, it is shortly but adequately demonstrated the interrelationship between the model state and parameters. Primarily, as indicated in Algorithm 2.1, the water infiltration state (Q_{inf}) is calculated as a function of the cover layer water content (θ), the model parameter set (Θ), and the meteorological forcing data set (u). This can be expressed as follows:

$$Q_{inf} = f(\theta, \Theta, u) \quad (56)$$

In turn, equations (16) and (19) show that the mobile and immobile water amounts in the waste body are estimated based on the water infiltration state (Q_{inf}), the model parameter set (Θ), and the meteorological forcing data set (u). By abuse of notation, these considerations are given as such:

$$V_M = f(V_{IM}, Q_{inf}, \Theta, u) = f(V_{IM}, Q_{inf}, \theta, \Theta, u) \quad (57)$$

$$V_{IM} = f(V_M, Q_{inf}, \Theta, u) = f(V_M, Q_{inf}, \theta, \Theta, u) \quad (58)$$

After all, it is clearly visible that the water balance model states Q_{inf}, V_M, V_{IM}, θ, and in turn, q_{cum} and $q_{discharge}$, and the model parameters Θ are interconnected as equations (56), (57) and (58) illustrate.